frontiers | Frontiers in Environmental Science

TYPE Original Research
PUBLISHED 04 April 2023
DOI 10.3389/fenvs.2023.1175957

OPEN ACCESS

EDITED BY
Marcus Vinícius Tres,
Federal University of Santa Maria, Brazil

REVIEWED BY
João Henrique C. Wancura,
Federal Institute of Rio Grande do Sul (IFSul), Brazil
Carolina Elisa Demaman Oro,
Universidade Regional Integrada do Alto Uruguai e das Missões, Brazil
Maicon Sérgio Santos,
Federal University of Santa Maria, Brazil

*CORRESPONDENCE
Tutuk Djoko Kusworo,
tdkusworo@che.undip.ac.id

SPECIALTY SECTION
This article was submitted to Water and Wastewater Management, a section of the journal Frontiers in Environmental Science

RECEIVED 28 February 2023
ACCEPTED 27 March 2023
PUBLISHED 04 April 2023

CITATION
Kusworo TD, Kumoro AC, Aryanti N, Lingga FF, Widiastuti A, Vetcher AA and Dalanta F (2023), Development of anti-foulant ultraviolet-assisted polyvinyl alcohol layer on the polysulfone-based nanohybrid membrane for industrial rubber wastewater decontamination. *Front. Environ. Sci.* 11:1175957. doi: 10.3389/fenvs.2023.1175957

Development of anti-foulant ultraviolet-assisted polyvinyl alcohol layer on the polysulfone-based nanohybrid membrane for industrial rubber wastewater decontamination

Tutuk Djoko Kusworo[1]*, Andri Cahyo Kumoro[1], Nita Aryanti[1], Fadhilah Fatma Lingga[1], Ade Widiastuti[1], Alexandre A. Vetcher[2,3] and Febio Dalanta[1]

[1]Department of Chemical Engineering, Faculty of Engineering, Diponegoro University, Semarang, Indonesia, [2]Peoples' Friendship University of Russia (RUDN), Moscow, Russia, [3]Complimentary and Integrative Health Clinic of Dr. Shishonin, Moscow, Russia

Introduction: Membrane fouling has been reported to be one of the bottlenecks of membrane technologies for wastewater treatment. To mitigate its negative impacts, we fabricated polysulfone membrane (PSf) composites made of silica (SiO_2) and graphene oxide (GO) nanoparticles that modified with ultraviolet (UV)-assisted polyvinyl alcohol layer on the membrane surface.

Methods: The membrane composite was synthesized using non-solvent induced phase separation (NIPS) method. The membrane was further treated by UV irradiation and cross-linked with PVA coating to cope with the fouling problem. The modified membrane was applied for industrial rubber wastewater decontamination.

Results: The UV irradiation and cross-linked PVA coating to the PSf/GO-SiO_2 membrane improved the pseudo-steady state permeate flux by 60.15% from 20.05 to 50.32 L/m^{2}hr and maintained the permeate flux up to 82.33%. About 85% of total dissolved solids (TDS), 81% of chemical oxygen demand (COD), and 84% of ammonia compound (NH_3) with initial concentrations of 335.76, 242.55, 175.19 mg/L, respectively, could be removed after 8 h of membrane treatment. The modified membrane also exhibited an excellent flux recovery ratio of up to 83%.

Discussion: The modified membrane changed the fouling mechanism from pore blockage to cake filtration, which signifies the capability of the membrane to tackle

Abbreviations: ΔP, Trans-membrane pressure (Pa); A, Effective membrane area (m^2); C_f, Concentration of the pollutant in feed (mg/L); C_p, Concentration of the pollutant in permeate (mg/L); GO, Graphene oxide; J, Permeate water flux (L/m^{2}hr); J_0, Pure water flux for a clean membrane (m^{-1}s^{-1}); J_C, Water flux after cleaning (L/m^{2}hr); J_f, Pure water flux for the fouled membrane (m^{-1}s^{-1}), J_W, Initial water flux (L/m^{2}hr); K_b, Fouling constant for pore blockage; K_c, Fouling constant for cake filtration; K_i, Fouling constant for intermediate blockage; K_s, Fouling constant for standard blockage; PSf, Polysulfone; PVA, Poly(vinyl) alcohol; R, Rejection efficiency (%); R_f, Fouling resistance (m^{-1}); R_m, Intrinsic membrane resistance (m^{-1}); R_T, Total membrane resistance (m^{-1}); SiO_2, Silicon dioxide; SSE, Sum of squared errors; SSR, Sum of squared residuals; t, Filtration time (hr); UV, Ultraviolet; V, Volume of the permeate (L); μ, Dynamic fluid viscosity (Pa.s).

severe fouling tendency. The cross-linked UV/PVA coating reduced fouling formation by reducing the adsorptive interactions between the foulant molecules and the membrane surface by enhancing membrane surface hydrophilicity. This implies that incorporating GO/SiO_2 nanoparticles with UV irradiation and PVA coating substantially enhanced the physicochemical properties of the PSf membrane.

KEYWORDS

nanohybrid membrane, PVA coating, UV irradiation, antifouling properties, fouling mechanism, industrial rubber, wastewater treatment

1 Introduction

Natural rubber products have emerged as an important material due to their outstanding properties in terms of elasticity and strength than the synthetic rubber products. The increase in production activity in the rubber industry generates a higher volume of wastewater which contains various organic and inorganic contaminants. The rubber industry usually discharges 25 m^3 of wastewater for each metric ton of raw rubber suspension, which is so-called natural rubber-laden wastewater (NRW) (Habashi et al., 2016). The contained hazardous dissolved contaminants such as micro rubber particles, organic matter, and ammonia compounds (NH_3-N) are the ultimate problem makers of this wastewater (Habashi et al., 2016). Conventionally, NRW is processed using a combination of aerobic and anaerobic ponds as well as a combination of coagulation and flocculation processes (Zhao et al., 2021). Nevertheless, these methods require further separation systems and large processing areas, thus, increasing operating and maintenance expenditures. Moreover, conventional methods commonly have low separation performance for dissolved organic matter and NH_3-N (Habashi et al., 2016). Therefore, it becomes a particular interest to develop a method that can provide a sophisticated separation performance, compact process system, and low operating expenditure.

Recently, due to its ease of technical applicability, sophisticated separation performance, and compact design, membrane technology has been massively performed for wastewater treatment purposes worldwide (Vinardell et al., 2020; Zolghadr et al., 2021). Some benefits from the implementation of membrane technology in wastewater treatment have been demonstrated, including, clean process, low energy consumption, compact design, less chemical consumption, versatility to be combined with other processes, tunable removal properties, and sludge-free (Hu et al., 2020; Sharma et al., 2020; Vinardell et al., 2020; Younis et al., 2020; Álvarez Bayona et al., 2022). Despite its superiority, the membrane filtration process is prone to fouling issues (Zhao et al., 2020). When contaminants are attached to the membrane's pore or surface, fouling develops, which lowers the permeate flow and selectivity (Zhao et al., 2020). Fouling on the membrane can be promoted by physical interaction such as shear force or drag permeation and by chemical interaction such as ion binding effects and hydrophobic interactions (Liu et al., 2020; Zhao et al., 2020). Numerous efforts have been paid to reduce membrane fouling; polyelectrolyte multilayer is an example of a fouling reduction approach in nanofiltration membranes (Evdochenko et al., 2021). Another study demonstrated that membrane fouling can be controlled by embedding hydrophilic materials (nanoparticles or polymers) into a polymeric membrane (Dmitrenko et al., 2021; Evdochenko et al., 2021; Li F. et al., 2021). Group of hydrophilic polymers, including polyethylene glycol (PEG), polyvinyl alcohol (PVA), polyvinyl pyrrolidone (PVP), polymethyl methacrylate (PMMA), polyacrylic acid (Chiao et al., 2020), polyelectrolytes, and others for surface coating of the membrane has been used to tackle fouling formation on the membrane surface (Liu et al., 2021; Vaysizadeh et al., 2021; Wang et al., 2021; Wanke et al., 2021). Inorganic nanosized metal oxides have also been demonstrated to have outstanding antifouling properties, such as iron oxide (Fe_3O_4) (Chai et al., 2020), zirconium oxide (ZrO_2) (Rambabu et al., 2020), aluminum oxide (Al_2O_3), zinc oxide (ZnO) (Vatanpour et al., 2020), silicone dioxide (SiO_2) (Nguyen et al., 2021), graphene oxide (GO) (Fan et al., 2021), and titanium oxide (TiO_2) (Nguyen et al., 2020).

Due to its excellent thin sheet strength, ease of dispersion in water or organic solvents, and high compatibility with a ceramic or polymer matrix, graphene oxide (GO) was chosen in this work as a membrane filler (Kusworo et al., 2021b). GO-based nanocomposites have been utilized to develop outstanding membrane composites by co-incorporating with Fe_3O_4, TiO_2, and ZnO (Chai et al., 2020; Tran et al., 2020; Kazemi et al., 2021). It has been found that the permeate flow recovery of the PSf-Fe_3O_4/GO composite membrane possessed 95% that reasonably promoted by the synergetic works of Fe_3O_4 and GO in the membrane composite that enhances permeability, pollutant elimination, and antifouling properties of the membrane (Chai et al., 2020). Moreover, it has been observed that the nanohybrid TiO_2/GO PVDF membrane possessed remarkable performances in terms of flux, rejection, and antifouling tendency due to the photocatalytic properties of the TiO_2/GO nanocomposite (Tran et al., 2020). Functionalization of GO with other chemical groups has been reported to improve some properties of GO such as silylated GO for dispersibility improvement (Ganguly et al., 2019), Ag decorated rGO for a catalytic process (Das et al., 2018), CeO_2-PrGO for phosphate reduction (Bakry et al., 2022), and candle waste micro-encapsulates modified GO for hydrophilicity enhancement (Younes et al., 2023). Kazemi and coworkers reported that a nanohybrid PVC/GO-ZnO membrane that co-incorporating ZnO and GO can decrease the risk of fouling and can flawlessly maintain a consistent permeate flow at 120 L/m^2hr (Kazemi et al., 2021). Based on the aforementioned results of the study, the co-incorporation of GO and inorganic metal oxides significantly enhanced the overall performance of the membrane. Therefore, it

was expected that the synergistic effect of SiO_2 and GO might also promote better membrane performance. Several cases of nanohybrid membrane utilization for wastewater treatment with a high organic pollutant content have caused a relatively short lifetime due to fouling formation on the surface of the membrane (Kazemi et al., 2021). It is also promoted by the gradual reduction of surface hydrophilicity (Younas et al., 2019; Zabihi et al., 2020; Wanke et al., 2021). Conclusively, the co-incorporation of GO and SiO_2 is just not enough to have longer hydrophilicity and antifouling property. Therefore, other brilliant ideas are needed to overcome this classic issue in membrane filtration applications.

Irradiating the membrane sheet under ultraviolet (UV) light was expected to overcome the fouling problem on the membrane's surface. It was also expected to prevent the unselective-voids formation in the membrane. The UV light exposure on the membrane has been reported to improve the hydrophilicity of the nanohybrid membranes by initiating the carbonyl and hydroxyl groups generation that results in a high permeate flux as well as an improvement in pollutant rejection (Zabihi et al., 2020). UV irradiation is also effective to create the crosslinking pattern on the polymer backbone (Scalia et al., 2019). Further, UV irradiation was reported that can enhance the thermal and mechanical properties of the polymer (Rao et al., 2019). This method can also be used for tuning the desired pore size in the membrane. Another idea to improve the hydrophilicity and antifouling properties of the membrane is by coating the membrane's surface using a stable and highly hydrophilic chemical such as polyvinyl alcohol (PVA) (Lu et al., 2021). It was reported that the crosslinked PVA significantly minimizes the existence of hydrophobic foulants, improving membrane resistance (Lu et al., 2021). PVA-coated polyamide membrane was noticed that the covalent bonding of PVA can enhance hydrophilicity, slightly increase surface roughness, and enhance permeate flux and pollutant removal (Bai et al., 2020). Coating with cross-linked PVA can also enhance the crystallinity of the polymeric membrane by cross-linking between molecules of the membrane (Lu et al., 2021). As a polymer coating agent, PVA has the ability to increase the membrane's anti-fouling property and remove the unselective gaps by covering the spaces present between the polymer matrix and the surface of the nanoparticle (Zhong et al., 2021). The combination of UV light irradiation and PVA coating on the PSf/GO-SiO_2 membrane surface becomes a particular research interest as an effort to solve the classic fouling problem on the membrane's surface.

The natural rubber-laden wastewater from the industry generated extraordinarily high volume and high emerging pollutant content; hence, it needs a reliable, cost-effective, simple, and durable treatment method. The applications of membrane technology on numerous types of water and wastewater treatment have been unquestionably proven with outstanding results (Chaumien et al., 2012; Bell et al., 2017; Zhan et al., 2019; Jain et al., 2020; Kusworo et al., 2021a). To present the novelty, this current study focuses on the integrated UV light irradiation and PVA coating on the nanohybrid PSf/GO-SiO_2 membrane for efficient natural rubber-laden wastewater treatment, which has not yet been studied. To put more worth in this study, fouling evaluation was performed by using four different fouling models. This fouling evaluation can be comprehensively assessed and identified the major fouling mechanisms that occurred on the membranes. The effects of surface modification of the membranes on fouling mitigation were also investigated. Specifically, this paper discusses the effect of UV exposure prior to the coagulation and PVA coating on the membrane surface to enhance the membrane performance and antifouling properties.

2 Materials and methods

2.1 Materials

Polysulfone (PS 99%f) UDEL® PSU P-1700 NT was obtained from Solvay Advanced Material (US). *N*-methyl 2-pyrrolidone (NMP) was supplied by Merck (Indonesia). Silicon dioxide (SiO_2, 99%) nano powder was obtained from Nano Center, Indonesia. Graphite powder (Graphite, 99.5%) was obtained from Mada Kimia Indonesia that was used to synthesize graphene oxide (GO) by adapting the modified Hummer's method. Sulfuric acid (H_2SO_4, 98% v/v), potassium permanganate ($KMnO_4$, 99%), and hydrogen peroxide (H_2O_2, 30% v/v) were obtained from Merck, Germany. Polyvinyl alcohol powder (PVA, MW 30–70 kg mol^{-1}, 89% w/w) was obtained from Wako Chemical, Japan. Natural rubber industry wastewater (secondary treatment discharge) was collected from PTPN VII (Bengkulu, Indonesia). The detailed contaminant parameters of the wastewater are listed in Supplementary Table S1.

2.2 Synthesis of graphene oxide (GO)

GO was synthesized based on the modified Hummer's method (Vazquez-Jaime et al., 2020). Graphite powder (2 g), H_2SO_4 (240 mL), and H_3PO_4 (26.7 mL) were mixed and stirred for 10 min. Afterward, $KMnO_4$ (11.7 g) was slowly introduced to the mixture, and stirring continued for 6 h until the formation of a dark green solution. About 6 mL of H_2O_2 was added dropwise, while simultaneous stirring was extended for 10 min. Subsequently, the solution was equilibrated to room temperature (~25°C). About 90 mL of HCl was added slowly to the solution under continuous stirring. Finally, approximately 266 mL of deionized (DI) water was slowly added to the mixture. The resulting solution was centrifuged at 5,000 rpm for 5 min to separate the supernatant and the precipitate. The supernatant was discarded, while the precipitate was repeatedly washed with a washing solution, prepared by mixing 10 mL of HCl and 5 mL DI water. Upon centrifugation, the precipitate was dried at 90°C for 24 h in an oven.

2.3 Synthesis of nanohybrid PSf/GO-SiO_2 membrane

Non-solvent induced phase inversion (NIPS) method was used in the preparation of membranes (Dalanta et al., 2022). For fabricating the neat PSf membrane, PSf (17 wt%) is used as the polymer content that dissolved in NMP. The solution was further stirred (Labinco L71, Labinco BV, Netherlands) at 350 rpm until achieving a homogenous solution, and the resulting membrane solution was degassed using an ultrasonic bath. The polymer solution was cast onto a clean glass plate.

The membranes were cast using a casting knife, and the casted solution was immersed in the DI water bath at 30°C for 24 h, to form the membrane sheet. For the PSf/GO membrane, the GO with a concentration of 0.5 wt% was mixed with the PSf membrane dope solution and sonicated for 1 h until they were completely dispersed to prevent aggregation. The same method was applied to make a PSf/SiO_2 membrane with a SiO_2 concentration of 0.5 wt%. To fabricate PSf/GO/SiO_2 membrane, firstly 0.5 wt% of GO and 0.5 wt% of SiO_2 were mixed into 50 mL of PSf dope solution. The membrane solution was then continuously stirred at 350 rpm for 12 h to obtain a homogeneous membrane solution. The resulting solution was cast onto a clean glass plate and coagulated using DI. The glass plate was horizontally immersed in DI water at 30°C overnight to completely remove the residual solvent, facilitating the solidification of a membrane structure. The fabricated membrane was dried for 24 h at room temperature (~25°C).

2.4 Integrating UV irradiation and cross-linked PVA coating of PSf/GO-SiO_2 membranes

Irradiating UV rays and PVA coating were selected for surface modification of the membrane. The surface modification of the membranes using UV irradiation was conducted by following this procedure. Firstly, the casted polymer solution on the glass plate was subjected to UV lamp typed C (265 nm) with three variations (1; 3; and 5 min). Then, to produce the membrane sheets, the same method of NIPS was performed as explained in Section 2.3. This method resulted in the modified membranes with UV irradiation. Subsequently, to further modify the surface property of the membrane, PVA coating was employed. The modified membranes by UV irradiation by the previous step were further coated using various PVA concentrations (0.5; 1; and 2 wt%). A predetermined mass of PVA was dissolved in DI water at 70°C–80°C. The solution was stirred at room temperature until attaining a homogeneous mixture. Then, the top side of the membrane was carefully dipped into PVA solution for 60 min. The excess PVA solution was wiped and then the membrane was dried in a vacuum oven at 40°C for 120 min. The dried coated membranes were further immersed into the cross-linking solution at room temperature (~25°C) for 2 h. The cross-linking solution contained 5 wt% of glutaraldehyde as the crosslinking agent and sulfuric acid 0.5 wt% as the catalyst. The membranes were then washed using DI water to remove the remaining residue of the cross-linking agent. Finally, the membranes were left at room temperature (~25°C) for 24 h to be dried.

2.5 Membrane characterization

A scanning electron microscope (SEM) JSM-6510-LA (JEOL, Tokyo, Japan) was utilized to observe the cross-section and surface morphology of the fabricated membranes. The membrane morphologies were scanned at × 1,000 and × 5,000 magnifications for the cross-section and surface observation, respectively. Prior to SEM analysis, the membrane samples were soaked in liquid N_2 to improve their brittleness. Afterward, the samples were cut into desirable forms and coated with gold. Functional groups of the membranes were determined before and after surface modification using FTIR (Perkin Elmer Frontier, United States) apparatus. The absorbance of the functional groups that existed in the membrane samples was observed in the wavenumbers ranging from 4,000–400 cm^{-1}. A dynamic contact angle meter (RASE, Japan) was used to measure the surface hydrophilicity of the fabricated membranes. Moreover, the mechanical properties of the membranes in form of tensile strength and elongation at break were investigated using a material testing instrument (UTS HOO1, China). The measurement of membrane porosity was carried out using the immersion method, with the detailed method from our previous work (Arifeen et al., 2019). The Gueroult-Elford-Ferry equation is used to determine the average pore size of the fabricated membranes, by following the method reported by (Younas et al., 2019). The method for calculating water uptake and membrane affinity was adapted from (Kusworo et al., 2021b). Further, the membrane's affinity towards liquid was measured using a theoretical Flory-Huggins model.

2.6 Flux and pollutant rejection evaluation of fabricated membranes

The membrane permeation flux was investigated using a laboratory-scale cross-flow filtration system (Supplementary Figure S1). The feed spacer and the membrane coupon were mounted to the filtration cell. Prior to wastewater flux analysis, the membrane was acclimated using deionized water for 30 min. This test was performed at an operating pressure of 5 bar trans-membrane pressure with a membrane area of 12.57 cm^2. The permeate flux was recorded every 30 min for 5 h for each membrane. The membrane water flux values were then calculated using Eq. 1.

$$J = \frac{V}{A \times t} \tag{1}$$

Where J and V are the permeate water flux (L/m^2hr) and the volume of the permeate (L), while A and t are effective membrane area (m^2) and filtration time (hr), respectively.

The TDS concentration was quantified using a TDS meter type HI98301 DiST 1 (Hanna Instruments, United States), while the COD was measured spectrophotometrically using the dichromate method. Accordingly, ammonia (NH_3-N) concentration was quantified using Nessler's reagent by UV-vis spectrophotometer. Eq. 2 was employed to quantify the pollutant rejection.

$$R = \left(1 - \frac{C_p}{C_f}\right) \times 100\% \tag{2}$$

Where R is rejection efficiency (%), while C_p and C_f are the concentration of the pollutant in permeate and feed solution, respectively (mg/L).

2.7 Membrane's antifouling ability and resistance analysis

Pure water permeation of clean and fouled membranes was used to determine the fouling resistance. Darcy's equation, as shown in Eq. 3, was used to calculate the intrinsic membrane resistance (Kusworo et al., 2021b)

$$R_m = \frac{\Delta P}{\mu J_o} \quad (3)$$

Where R_m is the intrinsic membrane resistance (m^{-1}), ΔP is the trans-membrane pressure (Pa), μ is the dynamic fluid viscosity (Pa.s), and J_0 is the pure water flux for a clean membrane ($m^{-1} \times s^{-1}$). The fouled membrane was rinsed using DI water and soaked for 24 h at room temperature (~25°C). Subsequently, DI water permeation tests of the fouled membranes were performed employing the same operating conditions that were used for clean membrane tests. The fouling resistance (R_f) was determined using Eq. 4 (Kusworo et al., 2021b).

$$R_f = \frac{\Delta P}{\mu J_f} - R_m \quad (4)$$

Where R_f is the fouling resistance (m^{-1}), J_f is the pure water flux for the fouled membrane ($m^{-1} \times s^{-1}$). The total membrane resistance (R_T) was determined using Eq. 10 (Kusworo et al., 2021b).

$$R_T = R_m + R_f \quad (5)$$

Where R_T is total membrane resistance (m^{-1}).

To analyze the antifouling properties of the membrane, the flux recovery ratio (FRR) was evaluated. The antifouling performance of the membranes was investigated by continuous filtering of the distilled water and rubber solution to the membrane for 120 min at 1 bar to ensure that the water flux (J_w) reaches a stable stage. Natural rubber-laden wastewater treatment was filtered for 120 min at the same pressure (1 bar). After the filtration was completed, the membranes were repeatedly washed with DI water for 15 min. Finally, the pure water flux of cleaned membranes (J_C) was measured. The FRR was determined by applying Eq. 6 (Younas et al., 2019).

$$FRR = \frac{J_c}{J_w} \times 100\% \quad (6)$$

Where J_W is water flux, while J_C is water flux after cleaning.

2.8 Evaluation of fouling mechanisms of the fabricated membranes

To investigate the formation mechanism of fouling on the fabricated membranes, four different models were used, namely, the complete-standard model, intermediate-standard model, cake-complete model, and cake-intermediate model, as shown in Eqs 7–10, respectively (Bolton et al., 2006). The complete-standard model assumes that two separate fouling mechanisms occur independently throughout the duration of the run (Bolton et al., 2006). This can occur if small particles cause the membrane pores to become narrower, and caking is caused by larger particles on the membrane surface. The intermediate-standard model occurs when a membrane fouls by the combined complete or intermediate blocking mechanism with some parts of the pores no longer available for flow (Ho and Zydney, 2000). The combined cake-complete model assumes that fouling is caused by the independent effects of complete blocking and caking (Ho and Zydney, 2000). Lastly, the cake-intermediate model represents the combined caking layer and intermediate blocking that occurred in the membrane by foulants. This model combined the effects of caking and pore constriction (Bolton et al., 2006). These models were used to evaluate the main promoters of the occurred fouling on each membrane. The curve fitting method was used to find the proper model for each tested membrane. Statistical analysis of the sum of squared residuals (SSR) was employed to identify the fitting parameters. A lower SSR indicates a better fit of the model to the data, while a higher SSR suggests that the model may not be capturing all of the underlying patterns in the data (Silva et al., 2013). Therefore, minimizing the SSR is a common goal in statistical modeling and regression analysis.

$$V = \frac{J_0}{K_b}\left(1 - \exp\left(\frac{-2K_b t}{2 + K_s J_0 t}\right)\right) \quad (7)$$

$$V = \frac{1}{K_i}\ln\left(1 + \frac{2K_i J_0 t}{2 + K_s J_0 t}\right) \quad (8)$$

$$V = \frac{J_0}{K_b}\left(1 - \exp\left(\frac{-Kb}{K_c J_0^2}\left(\sqrt{1 + 2K_c J_0^2 t} - 1\right)\right)\right) \quad (9)$$

$$V = \frac{1}{K_i}\ln\left(1 + \frac{K_i}{K_c J_0}\left(\sqrt{1 + 2K_c J_0^2 t} - 1\right)\right) \quad (10)$$

Where V is the filtrate volume (m^3), J_0 is the initial permeate flux (m/s), t is the duration of filtration (s), K_b, K_s, K_c, and K_i are fouling constants that represent pore blockage, standard blockage, cake filtration, and intermediate blockage, respectively.

3 Results and discussion

3.1 Morphological characteristics and surface roughness of the fabricated membrane

The morphological characteristics of membranes are important to understand the membrane's permeability and selectivity. The SEM images of the unmodified and modified membranes are presented in Figure 1. Figure 1(a1) shows that the neat PSf membrane possessed a porous surface with some defects across its surface. Moreover, the neat PSf attributed finger-like structure and large void pores in the cross-section image, as shown in Figure 1(a2). The porous surface and large voids of the neat PSf were attributed to the unselective pollutant separation. Figures 1B, C presents the distribution of SiO_2 nanoparticles and GO nanosheets across the surface of the PSf/SiO_2 and PSf/GO membranes, respectively. However, the distribution of the nanoparticles was not uniform enough, as indicated by agglomerations and polymer clots on the membrane surface, leading to poor separation and low antifouling performance. On the other hand, Figure 1(d1) displays that the surface of the modified membranes was smoother than that of the neat PSf membrane, as no visible pores were observed. The cross-linked PVA coating represented a selective layer to repair the unselective void and improve the membrane surface hydrophilicity. Further, the thin PVA layer on the membrane can be observed in Figure 1(d2). The relatively similar size of the micro-void could increase the porosity of the membrane potentially enhancing water uptake ability and permeability. The cross-linked PVA-coated

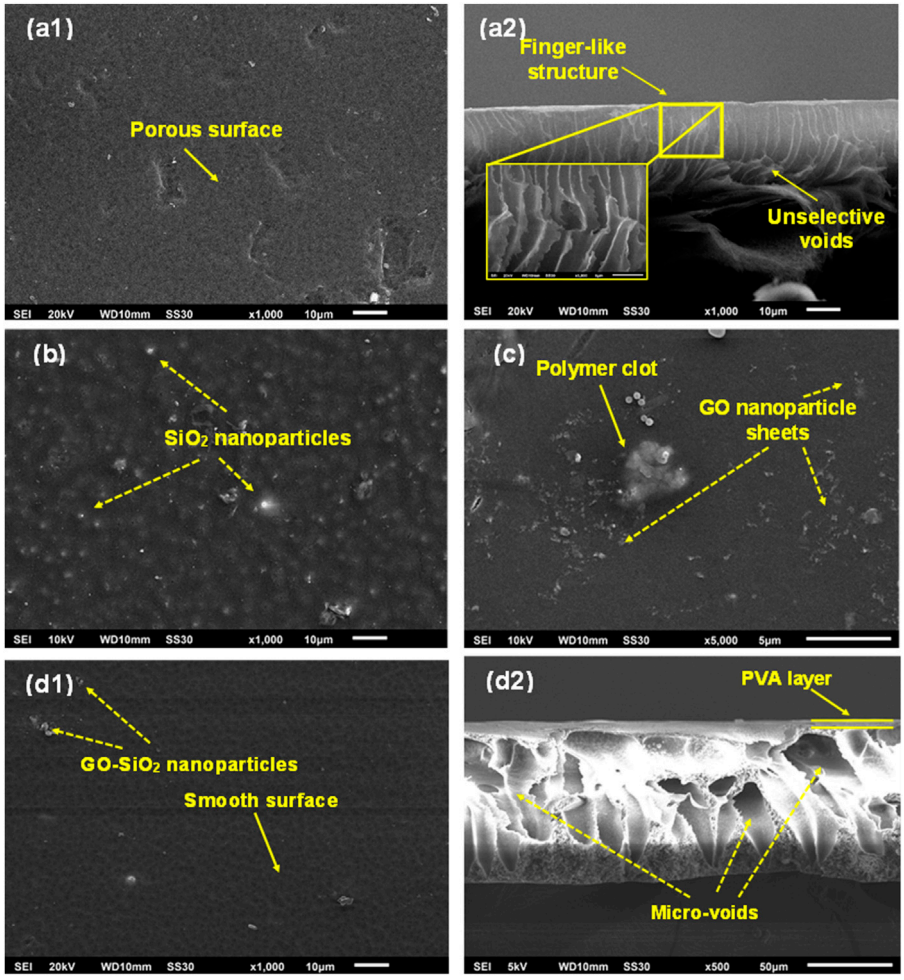

FIGURE 1
SEM images of fabricated membranes, **(a1)** Surface image and **(a2)** Cross-section image of neat PSf membrane, **(B)** Surface image of PSf/SiO_2 membrane, **(C)** Surface image of PSf/GO membrane, **(d1)** Surface image and **(d2)** Cross-section image of PSf/GO-SiO_2 membrane modified with UV/PVA.

membrane exhibited higher and more stable flux due to its higher hydrophilicity.

Nevertheless, the modified membrane suffered from surface defects (becoming rougher) due to the slight agglomeration of the GO/SiO_2 nanoparticles incorporated into the membrane matrix. This finding was in accordance with (Feng et al., 2021), who reported the same surface defect that occurred due to the presence of GO/SiO_2 nanoparticles, which were not uniformly dispersed in the dope solution. They suggested that casting this mixture on the glass would cause a slight scratch or defect on the membrane surface and also induce the formation of aggregates. In addition, many bubble-like shapes were exhibited on the membrane surface due to membrane compaction during drying, as the PVA was not homogeneously mixed with the GO/SiO_2 nanoparticles. This might be the cause of the formation of non-selective pores, which slightly reduced membrane selectivity. Nevertheless, the SEM analyses proved that the additions of GO/SiO_2 nanoparticles, irradiation of UV, and cross-linking PVA coating significantly improved the micromorphological structure of the membrane. Finally, the PSf/GO-SiO_2 modified with UV/PVA represented the most prominent membrane in terms of micromorphological structure that could provide the best filtration performance.

Figure 2 shows the surface roughness profiles of the fabricated membranes. Figure 2A depicts the roughness profile of the neat PSf membrane. It can be seen that this unmodified membrane has a rough surface that is reflected by the distribution of peaks across the surface. Further, the addition of nanoparticles results in an increase in roughness level. By comparing Figures 2B, C and Figure 2A, it is clearly observed that the addition of nanoparticles caused more formation of peaks on the membrane surface. The peaks strongly indicate the sites of nanoparticles that exist on the membrane surface. However, a rougher membrane surface seems to have a higher tendency to fouling formation (Horseman et al., 2021). Contaminants can be trapped between the rough sites of the membrane, whereas the fouling formation is undesirable. Interestingly, the PVA crosslinking coating was successful to generate a more uniform membrane surface, as shown in Figure 2D. The hydrophilic property of PVA can also increase membrane permeability (Hashino et al., 2011; Horseman et al., 2021). At the same time,

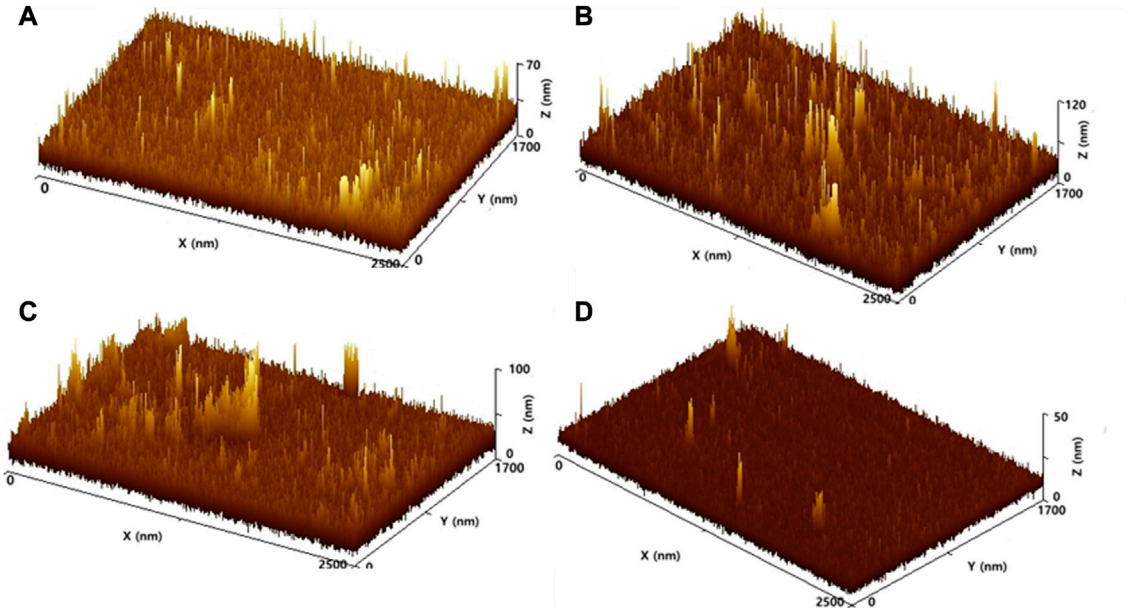

FIGURE 2
Surface roughness profiles of the membranes: **(A)** neat PSf, **(B)** PSf/SiO_2, **(C)** PSf/GO-SiO_2, and **(D)** PSf/GO-SiO_2—UV/PVA.

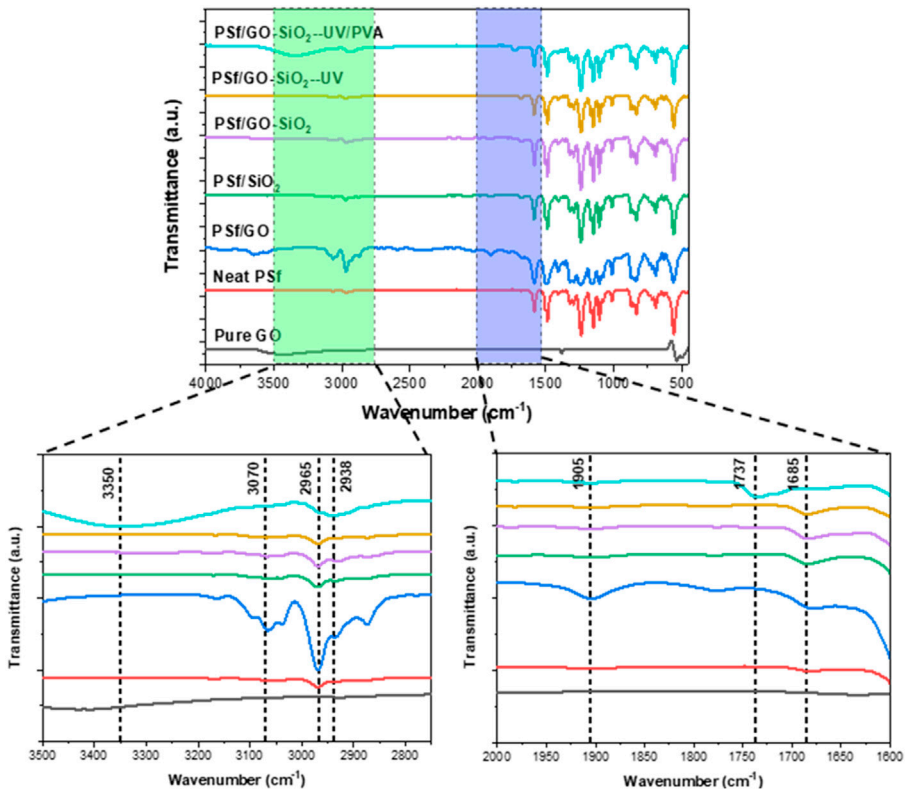

FIGURE 3
FTIR spectra of the fabricated membranes.

the uniform and less rough surface can provide a lower probability of fouling formation on the membrane surface, due to the fewer pore constrictions on the membrane surface. It can be concluded that the PVA coating on the membrane surface significantly improved the uniformity and reduced the surface roughness of the membrane.

TABLE 1 Pore properties including thickness, porosity, and pore size of the membranes.

Membranes	Thickness (μm)	Porosity (%)	Pore size (nm)
Neat PSf	70.32 ± 0.12	65.10 ± 0.22	43.76 ± 1.12
PSf/GO	72.41 ± 0.10	68.23 ± 0.28	35.14 ± 0.86
PSf/GO/SiO_2	79.55 ± 0.13	72.14 ± 0.46	30.45 ± 1.15
PSf/GO/SiO_2 –UV irradiation	81.06 ± 0.46	74.30 ± 0.50	38.23 ± 0.61
PSf/GO/SiO_2—UV/PVA	92.11 ± 0.58	75.00 ± 0.53	36.66 ± 0.33

3.2 FTIR spectra of the fabricated membranes

To evaluate the functional groups of the fabricated membranes, the FTIR analysis was performed, as the results are depicted in Figure 3. Figure 3 presents the GO nanoparticles with a typical FTIR spectrum that has some peaks corresponding to the oxygenated functional groups. A broad peak at 3350 cm^{-1} could be assigned to be the O-H stretching vibration and corresponded to a peak at 3070 cm^{-1}. The GO spectrum also shows a stretching vibration of the C=O group of aliphatic carboxylic acid at 1737 cm^{-1}, while the peak at 1685 cm^{-1} corresponded to the C=C stretching mode of GO sp^2. Another peak at 1401 cm^{-1} corresponded to the C-OH vibration (Chai et al., 2020; Fan et al., 2021). The absorption band of about 1250 and 1040 cm^{-1} was likely to be attributed to the stretching C-O-C group. When the GO/SiO_2 nanoparticles were incorporated into the membrane matrix, a new strong peak appeared at 1505 cm^{-1}, which could be attributed to the Si-O-Si stretching vibration of SiO_2 nanoparticles in the nanohybrid membrane. The more substantial peaks at 3400 cm^{-1} and 1640 cm^{-1} represented the existence of the -OH group of the GO/SiO_2 nanohybrid membrane (Wu et al., 2014; Nguyen et al., 2021). The peak enhancement could be associated with the formation of the hydrophilic GO/SiO_2 nanoparticles, which increased the -OH group and subsequently improved the hydrophilicity of the nanohybrid membrane. There was a slight difference in spectrum 1905 cm^{-1} ascribed to the C=O stretching vibration of aliphatic aldehyde, which intensified the interaction between nanoparticles and polymer matrix (Dehban et al., 2020; Shakak et al., 2020).

The higher availability of hydrophilic sites on the membrane, which is modified using UV irradiation and cross-linked PVA coating, could improve the permeability and antifouling properties of the membrane. The peaks at 3350 cm^{-1} and 3070 cm^{-1} were attributed to the hydroxyl group stretching GO flakes and PVA (Baroña et al., 2012; Medhat Bojnourd and Pakizeh, 2018). The broad peaks at 3350 cm^{-1} presented the–OH groups for membrane with cross-linked PVA coating and were assigned to the different–OH groups associated with the oxidation by-products of UV irradiation such as hydroperoxide (Baroña et al., 2012). Overall, the results of FTIR analysis confirmed that the integrated modification using UV irradiation and crosslinked PVA on the surface membrane could increase the hydrophilic properties.

3.3 Pore properties of the fabricated membranes

The porosity and pore size of the membrane is associated with the morphology of the membranes. According to Table 1, the membrane

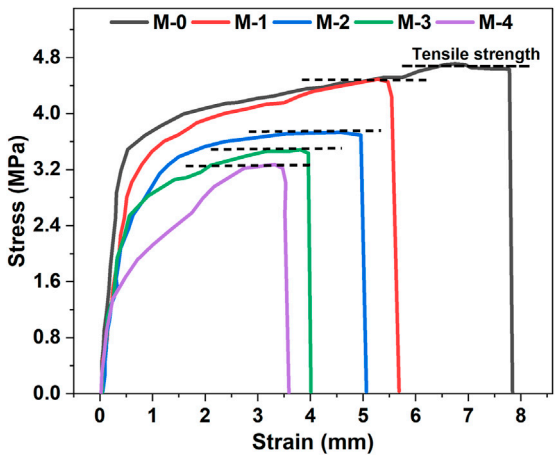

FIGURE 4
Stress-strain curves of the fabricated membranes.

thickness gradually increased due to the addition of nanoparticles, UV irradiation, and PVA coating treatment. The thickness of neat PSf was 70.32 ± 0.12 μm and reached 92.11 ± 0.58 μm in PSf/GO/SiO_2—UV/PVA membrane, resulting in an improved membrane porosity. Membranes with high porosity provided a higher permeate flux. A low porosity value indicated that the membrane was denser, while a high porosity value indicated the presence of a larger void space in the membrane. The presence of void space on the membrane structure was indicated by the value of membrane porosity. The addition of inorganic nanoparticles caused the formation of gaps inside the polymer matrix. With additional gaps present in the polymer, more voids were created and resulting in increased porosity. Additionally, in this measurement, we did a triplicate replication for each sample to represent the replicability of the method by applying the standard error. The standard error is a statistical measurement that quantifies the variability between samples drawn from the same population (Martínez et al., 2021). It is calculated as the standard deviation of the sample divided by the square root of the sample size. In other words, standard error measures how accurately the sample represents the population from which it is drawn. A smaller standard error indicates that the sample is a more accurate representation of the population, while a larger standard error indicates that the sample may not be as representative. It is important to note that standard error and standard deviation are not the same things. While standard deviation describes variability within a single sample, standard error

TABLE 2 Tensile strength and elongation at break of the fabricated membranes.

Code	Membranes	Tensile strength (MPa)	Elongation at break (%)
M-0	Neat PSf	4.72 ± 1.21	13.00 ± 0.90
M-1	PSf/GO	4.50 ± 0.73	9.50 ± 0.12
M-2	PSf/GO-SiO_2	3.72 ± 0.24	8.50 ± 0.43
M-3	PSf/GO-SiO_2–UV irradiation	3.51 ± 0.38	6.70 ± 0.50
M-4	PSf/GO-SiO_2—UV/PVA	3.28 ± 0.29	6.00 ± 0.14

describes variability across multiple samples of a population (Sugumar et al., 2022). Hence, the standard error is a crucial concept in statistical inference because it measures the accuracy with which a sample represents a population, and it helps to determine the level of confidence we can have in the results obtained from a sample.

3.4 Mechanical properties of the fabricated membranes

The mechanical properties of the membrane are important to show the robustness of the membrane in withstanding the varying conditions of the actual applications. In addition, these properties can be associated with the efficiency of the cleaning operation and the service life of the membrane. Figure 4 depicts the relationship between stress and strain of the fabricated membranes. Specifically, Table 2 summarizes the mechanical properties of the various modified nanohybrid membranes, as compared to the neat PSf membrane based on thickness, tensile strength, and elongation break. It was evident that the neat PSf (M-0) was the most amorphous polymer with poor chain compatibility in membrane formation. The neat PSf membrane was extremely stiff which caused weak interactions between the nanoparticles and the polymer matrix (Baroña et al., 2012). The mechanical characteristic of PSf/GO (M-1) was lower as compared to that of the neat PSf membrane. The incorporation of GO nanoparticles caused the tensile strength to decrease by 3.7% from 4.72 ± 1.21 to 4.50 ± 0.73 MPa, whereas the elongation at break also declined from 13% to 6%. The results indicated that the addition of GO nanoparticles to the membrane decreased the membrane's elasticity. This could be attributed to the aggregation of GO, which made the membrane polymer and GO nanoparticles blend stronger and more brittle than the neat PSf membrane.

The UV irradiation reduced the tensile strength of the membrane from 3.72 ± 0.24 MPa to 3.51 ± 0.38 MPa. The decreasing mechanical strength was mainly attributed to the surface crack and defect during photodegradation due to direct exposure to UV irradiation. Embrittlement also contributes to tensile properties. Embrittlement was caused by an oxidation reaction, chain-scission, and the decomposition of material during polymer degradation (Kusworo et al., 2021b). These decreased mechanical properties due to UV irradiation are caused by the combined effects of surface crack, defect, and embrittlement on the nanohybrid membrane. Moreover, the coating of cross-linked PVA on the nanohybrid PSf/GO-SiO_2 membrane (M—4) improved the mechanical properties of the nanohybrid membrane. This treatment resulted in the reduction of tensile strength and elongation at the break due to the excessive -OH groups. As a result, this created a rigid crystalline structure and declined the membrane's crystallinity. The incorporation of cross-linked PVA into the nanohybrid PSf/GO-SiO_2 membrane decreased the elongation at break and tensile strength of the membrane causing the membrane to become stiffer.

3.5 Membrane surface hydrophilicity, water uptake ability, and affinity toward water

As one of the essential parameters of the membrane characteristic, the water contact angle analysis was performed to observe the hydrophilicity of the membranes after being modified with various nanoparticles, UV irradiation, and PVA coating. The measured water contact angles, along with their water uptakes of fabricated nanohybrid membranes, are presented in Figure 5A (a). As depicted in Figure 5A, the contact angle of the neat PSf membrane was the highest, which indicated that the membrane had the lowest hydrophilicity. The incorporation of GO/SiO_2 nanoparticles into the PSf membrane decreased the contact angle from 75.42° to 67.75°. A similar observation was reported by Chai et al. (Chai et al., 2020), who found that the addition of hydrophilic materials such as GO and SiO_2 nanoparticles to the PSf membrane solution increased the membrane's hydrophilicity as indicated by the reduction of the water contact angle. Theoretically, the addition of hydrophilic nanomaterials also increased the roughness of the membrane surface and facilitated better contact between water and OH groups on the membrane surface and diffusion through the surface. Figure 5 also confirms that the membrane modification through UV irradiation and crosslinking with PVA increased its hydrophilicity. The contact angle of the membrane surface was reduced by UV irradiation in the presence of hydrophilic monomers. The UV-irradiated membrane had a contact angle of 66.42°. The exposure of the membrane polymer to UV irradiation could initiate bond scission or re-arrangement which led to the formation of a hydrophilic group and decreased the contact angle. UV irradiation also caused the membrane surface to become rougher with a lower water contact angle so that the membrane became more hydrophilic. The contact angle of the membrane with cross-linked PVA coating decreased from 67.75° to 35.17°. This is explainable due to the fact that membrane modification with cross-linked PVA resulted in the attachment of hydroxyl groups on the membrane structure, which enhanced the hydrophilicity of the membrane. This would affect membrane permeate flux due to improved penetration of water droplets into the nanohybrid matrix.

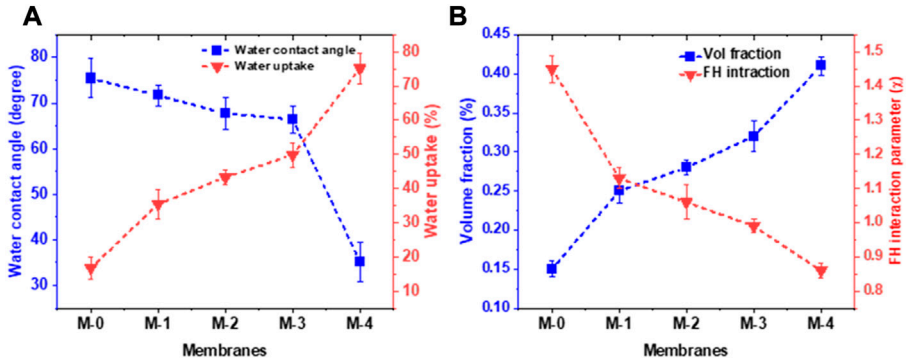

FIGURE 5
(A) Water contact angle and water uptake of the fabricated membranes and **(B)** membrane affinity towards water parameters, i.e., volume fraction and FH interaction parameter.

The attachment of hydroxyl groups in the membrane reduced the water contact angle and provided easier access for water molecules to pass through the membrane pores. The ability of cross-linked PVA to decrease the water contact angle can be associated with stronger dipole-dipole interactions between the cross-linked PVA and water molecules. Figure 5A also shows the water uptake of the fabricated membranes. It can be seen that the addition of GO-SiO_2 nanoparticles can enhance the water uptake ability from 18.35% in neat PSf to 43.21% in PSf/GO-SiO_2 membrane. The increase in water uptake can be caused by the synergistic effect of hydrophilicity and porosity properties of the membrane. The incorporation of GO-SiO_2 nanoparticles on the membrane was resulting in the higher hydrophilicity and porosity that makes the membrane can easily absorb the water molecules. Moreover, the surface treatment using UV irradiation and crosslinked PVA coating on the membrane was further increasing the water uptake characteristic. As previously discussed, UV and PVA coating treatments can enhance the hydrophilicity of the membrane, which also caused the strongest water uptake ability at a value of 75.32%.

Another interesting context regarding the membrane and water interaction behavior that can be studied is the affinity of the membrane toward the water. This particular phenomenon was evaluated by using a theoretical Flory-Huggins (FH) model. This model can further explain the sorption of water characteristics to the membrane matrix. The results of this study are presented in Figure 5B contains the volume fraction and FH interaction parameter of the tested membranes. The volume fractions were 0.15, 0.25, 0.28, and 0.41 for neat PSf (M-0), PSf/GO (M-1), PSf/GO-SiO_2 (M-2), and PSf/GO-SiO_2-UV/PVA (M-4), respectively. While, the FH parameters as the function of volume fractions were calculated at 1.45, 1.13, 1.06, and 0.86 for neat PSf, PSf/GO, PSf/GO-SiO_2, and PSf/GO-SiO_2-UV/PVA, respectively. This FH parameter can be used to explain the affinity between the membrane and water molecules. The lower value of the FH parameter indicates the higher sorption of water ability (Ganesh et al., 2013). The higher sorption of water can be leading to improvements in flux, pollutant rejection, and antifouling potential. The PSf/GO-SiO_2-UV/PVA shows the lowest value of the FH interaction parameter suggesting that the membrane ability after the addition of GO-SiO_2 and subsequent surface modifications can improve the membrane performance in a positive way.

3.6 Evaluations of the membrane performance

3.6.1 Effects of the GO and SiO_2 nanoparticles loadings on the performance of fabricated membranes

The addition of GO and SiO_2 nanoparticles to the PSf membrane is essential to improve the permeability and selectivity performance of the membrane. Figure 6A shows that the addition of GO nanoparticles to the PSf membrane improved the water permeate flux. Incorporating nanofillers would increase permeate flux due to the increased porosity and membrane hydrophilicity. The structure of micro-void pores with high porosity could lead to a decrease the mechanical strength, thereby affecting the long-term operation of the membrane. The same phenomenon can also be observed with the addition of SiO_2 nanoparticles. As displayed in Figure 5, the high hydrophilicity of the PSf membrane is due to the addition of 0.5 wt% SiO_2 nanoparticles increased the permeate flux of the membrane to 51 L m^{-2} h^{-1}. The SEM and FTIR analysis also confirmed that the addition of the nanoparticles induced defects and pore enlargement on the membrane surface due to its high crystallinity. However, the incorporation of SiO_2 nanoparticles was beneficial to improve membrane hydrophilicity. The presence of SiO_2 nanoparticles enlarged membrane pores with a finger-like structure, making the membrane become hydrophilic. When the membrane was used for filtration, the water molecules passed through the gaps quickly and improved the water permeate flux. Nevertheless, Figure 6B showed that the PSf/GO-SiO_2 membrane had poor flux stability, suggesting that the antifouling ability of the respective membrane was not good. The PSf/GO-SiO_2 membrane had approximately 70% flux reduction after 5 h of the filtration process. Hence, further modification is required to improve its flux stability.

Figure 6C presents the comparison of the rejection efficiency of the neat PSf, PSf GO, and PSf/GO-SiO_2 membranes. The addition of the GO nanoparticles significantly enhanced the organic pollutant

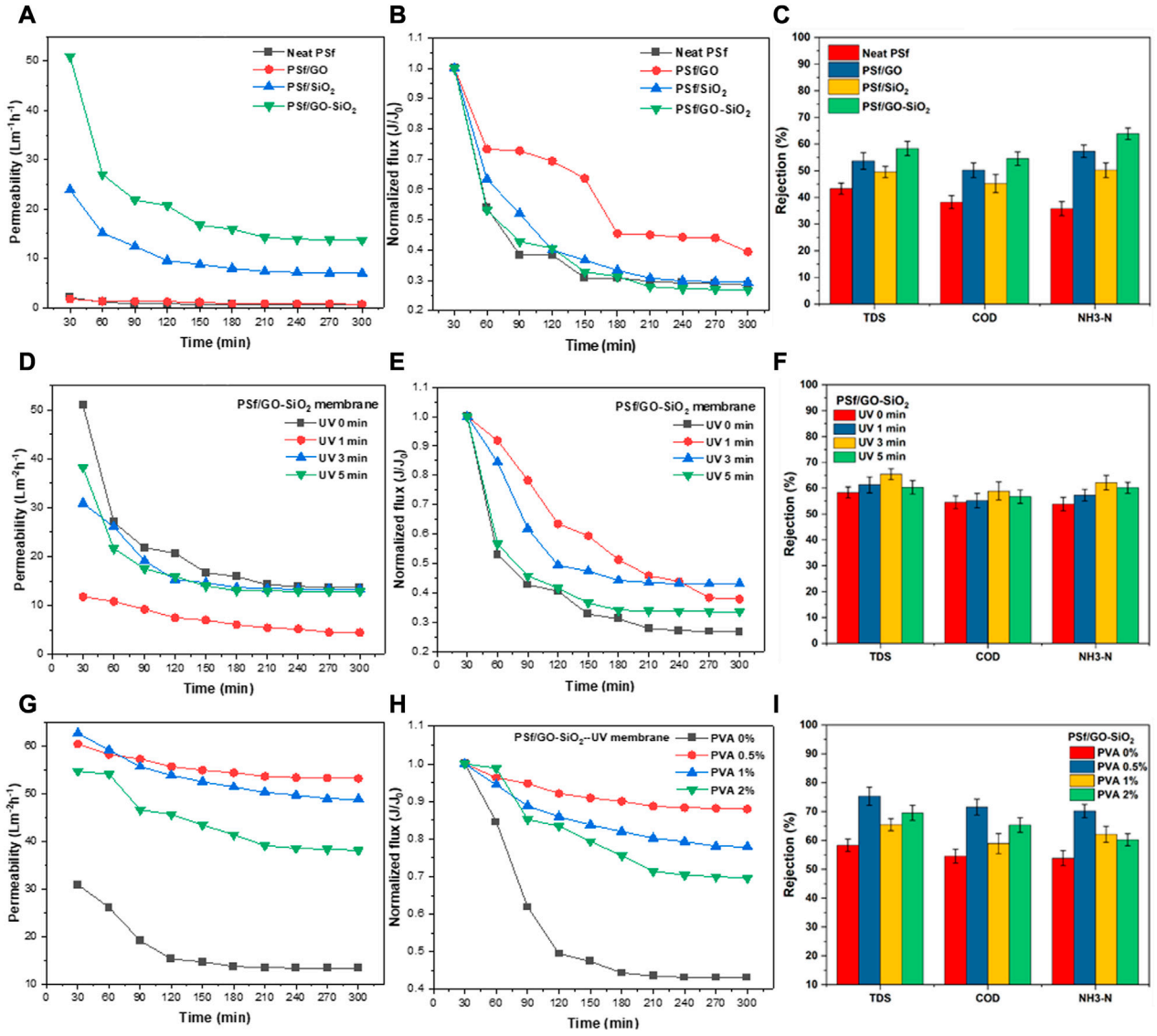

FIGURE 6
Effects of embedded nanoparticles on **(A)** Permeate flux, **(B)** Normalized flux results, and **(C)** Pollutant rejection performance. Effects of UV light treatment duration on **(D)** Permeate flux, **(E)** Normalized flux results, and **(F)** Pollutant rejection performance. Effects of PVA concentration on **(G)** Permeate flux, **(H)** Normalized flux results, and **(I)** Pollutant rejection performance on the tested membranes.

rejection percentages. In addition to the increasing hydrophilicity of the membrane, their incorporation as an inorganic filler enhanced the ionic adsorption and ionic retention through Donnan's exclusion mechanisms (Su et al., 2019; Alkhouzaam and Qiblawey, 2021). It can be seen that the addition of GO-SiO_2 showed the best rejection performance compared to the neat PSf, PSf/GO, and PSf/SiO_2. It is worth noting that PSf/GO-SiO_2 membrane removed 58.32, 54.54, and 63.86% of TDS, COD, and NH_3-N, respectively. This can be explained by the smaller pore size on PSf/GO-SiO_2 membrane compared to the other membranes. The smaller average pore size can perform more selective separation during filtration. Therefore, it can be concluded that GO-SiO_2 exhibited the best membrane filler compared to single GO or SiO_2. Similar results were reported by Ebrahimi et al. (2022), they found that incorporation of GO-SiO_2 nanoparticles into PAN membrane exhibited improved permeate flux by 78% and oil rejection by up to 98%, due to the formation of hydration layer that promotes hydrophilic layer and prevents contact between oil and membrane surface (Ebrahimi et al., 2022). Another benefit of GO-SiO_2 nanoparticles was observed by Mahdavi et al. (2022), they concluded that the incorporation of GO-SiO_2 into PVDF-g-PMMA membrane improved the permeate flux up to 64% and soybean oil rejection up to 93.4% (Mahdavi et al., 2022).

3.6.2 Effects of UV irradiation on the performance of PSf/GO-SiO_2 membrane

The UV irradiation of the membrane was proposed to improve the permeability and selectivity performance of the membrane as well as to help in fouling tendency reduction on the membrane's surface. Figure 6D presents that the membranes

exposed at longer durations of UV irradiation exhibited a higher permeate water flux. The membrane with 5-min exposure to UV irradiation had a larger initial permeate water flux of 38.06 L/m^{2}hr, as compared to those exposed to UV irradiation for 3 and 1 min, which only attained 32.96 and 13.73 L/m^{2}hr, respectively. These findings were in accordance with the porosity and pore size data presented in Table 1. This finding was also in good agreement with polymer chain degradation due to prolonged exposure of the membrane surface to UV light, which enlarged membrane pores and improved hydrophilicity and permeates flux (Gao et al., 2020). Motahari and coworkers reported that the permeability and selectivity of the membrane can be improved by performing UV irradiation. The tuned pore size of the membrane improved the selectivity of the membrane (Motahari and Raisi, 2020). In gas separation membranes, UV irradiation is usually used to enhance selectivity. Park and groups found that UV irradiation improved the selectivity in gas separation due to the crosslinking formation on the polymer backbone after experiencing UV irradiation (Park et al., 2020). The flux performance of the modified membrane using UV exposure had better stability (Figure 6E). The modified membrane using 3 min of UV exposure had the best flux stability among others, as it could maintain approximately 45% of flux stability after operating through 5 h of filtration. It is also found that UV light exposure for 3 min exhibited the best pollutant rejection compared to other duration. Under 3 min of UV exposure, the membrane can reject 65.44, 58.91, and 62.12% of TDS, COD, and NH_3-N, respectively, as shown in Figure 6F.

3.6.3 Effects of cross-linked PVA coating on PSf/GO-SiO_2 membrane performance

As the one of ultimate focuses of this study, the effects of PVA concentration as the coating solution on the flux and rejection profiles were evaluated. The performances of the cross-linked PVA-coated membranes are displayed in Figure 6G. Based on Figure 6G, along with the increasing PVA concentration in membrane coating, the permeate water flux also decreased. The initial flux of the coated membrane using PVA 2 wt% only reached 55.69 L/m^{2}hr, slightly lower than that of 1 wt% PVA-coated membrane, which attained an initial flux of up to 62.92 L/m^{2}hr. The best flux rate and most stable were achieved by the addition of 0.5 wt% of PVA which resulted in an initial flux of 60.09 L/m^{2}hr. Membrane with PVA coating had a finger-like structure with higher hydrophilicity being responsible for the higher water flux. In the previous study, cross-linked PVA coatings could reduce the contact angle, which corresponded with the increasing hydrophilicity of the membrane and result in an improved permeate water flux (Zhong et al., 2021). It was also found that the addition of PVA as a coating agent on the membranes improved the antifouling performance of the membrane.

As depicted in Figure 6H, the best PVA concentration to maintain the flux stability was attained by adding PVA 0.5 wt%, which could stabilize the permeate flux at 90% after 5 h of the filtration process. A higher concentration of PVA resulted in a higher polymer viscosity and caused the layer of the membrane coating to become slightly thicker. This inhibited water and reduced water penetration into the membrane matrix. Based on Figure 6I, shows that the best PVA concentration for membrane coating is 0.5%. When the higher PVA concentration was used, it seemed to have a reduction in pollutant rejection performance. A previous study reported that the addition of a hydrophilic polymer such as polymethyl methacrylate (PMMA) induced the formation of void structures thus increasing membrane porosity. The higher membrane porosity also occurred due to the changes in the polymer structure, which resulted in an intensive formation of porous structures (Younas et al., 2019). Therefore, a PVA concentration of 0.5% is considerably chosen as the best formulation for membrane coating that not only generates higher permeability but also higher pollutant rejection.

3.7 Evaluation of flux stability of the modified membranes

The flux stability test was performed by the initial flux test. The neat PSf and modified PSf membranes were examined for an 8 h long-filtration test under 5 bar of pressure for treatment of rubber-laden wastewater. The flux stability profiles of all membranes are presented in Figure 7. All of the membranes showed a flux decline along with the filtration time. The remarkable flux decline in the first-hour filtration run might be due to the membrane compaction and external fouling caused by specific compounds' attachment on the nanohybrid membrane surface. As shown in Figure 7A, the permeate flux declined from the initial flux until achieving a pseudo-steady state of 0.53, 0.55, 18.98, 20.05, and 50.32 L/m^{2}hr, for neat PSf, PSf/GO, PSf/SiO_2, PSf/GO-SiO_2, and PSf/GO-SiO_2—UV/PVA, respectively. Figure 7B also shows that the best flux stability of the membrane was found for PSf/GO-SiO_2—UV/PVA, which could maintain flux stability at approximately 82% after 8 h of filtration. On the other hand, the lowest permeate flux exhibited by the neat PSf membrane could be attributed to its lowest porosity and hydrophilicity which led to the lowest water mass transfer rate through the membrane sheet. The incorporation of GO-SiO_2 nanoparticles into the PSf helped to increase permeate flux due to the improvement of membrane hydrophilicity and porosity.

The combined UV irradiation and cross-linked PVA coating significantly increased the permeate flux up to 880%. However, the uncoated PVA membranes showed a significant flux decline at the first 2 h of filtration due to the external fouling. This can be explained due to the fact that a rougher membrane surface had a higher tendency to foulant attachment (Younas et al., 2019). Fouling that formed during membrane application blocked the tiny pores, thereby decreasing the membrane flux. The membrane with cross-linked PVA coating exhibited a high and stable flux due to the presence of a hydrophilic PVA layer that smoothened the rougher surface of the nanohybrid membranes. This was supported by the fouling resistance evaluation, of which the PVA-coated membrane had the lowest fouling resistance, as compared to the other membranes. In comparison with a previous study in the literature, Zhao et al. (2023) found that PVA coating is conducive to generating a smooth surface structure, and thus can promote uniform permeability and selectivity of the membrane (Zhao et al., 2023). A similar result was also found by Li et al. (2022) that a combination of PVA with CNT/TFC membrane

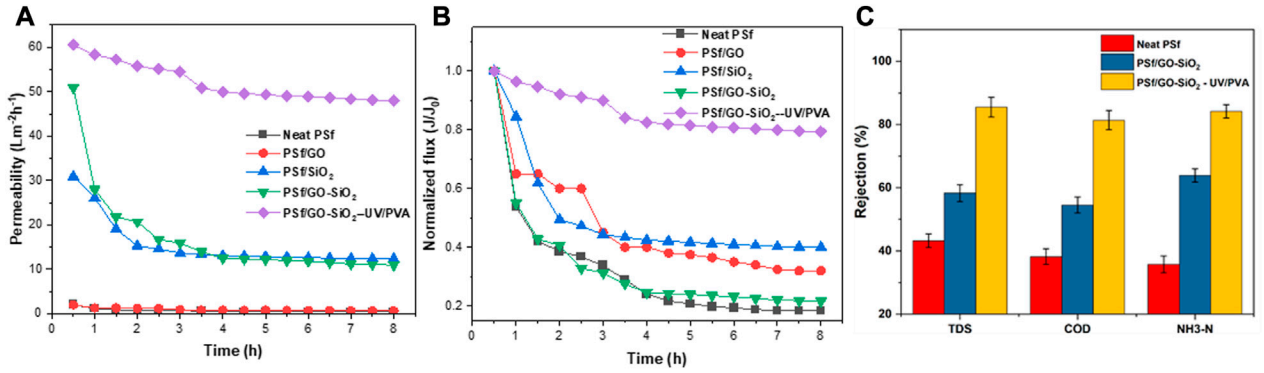

FIGURE 7
Membrane flux stability test for rubber-laden wastewater treatment **(A)** Profile of flux, **(B)** Normalized flux during 8 h of filtration, and **(C)** Pollutant rejections performance of the tested membranes.

TABLE 3 Membrane resistances during filtration.

Membranes	$R_m \times 10^{-10}$ (m^{-1})	$R_f \times 10^{-10}$ (m^{-1})	$R_T \times 10^{-10}$ (m^{-1})
Neat PSf	13.40 ± 0.18	31.28 ± 3.10	44.69 ± 4.50
PSf/GO	12.10 ± 0.15	14.62 ± 0.94	26.72 ± 1.60
PSf/SiO_2	0.69 ± 0.12	0.88 ± 0.36	1.57 ± 0.12
PSf/GO-SiO_2	0.42 ± 0.10	0.79 ± 0.12	1.21 ± 0.08
PSf/GO-SiO_2—UV/PVA	0.34 ± 0.08	0.16 ± 0.05	0.50 ± 0.11

exhibited just a slight flux reduction with 97% of flux recovery (Li et al., 2022). The developed membrane composite was also excellent in mechanical strength. Overall, those finding indicates that cross-linked PVA coating on nanohybrid membrane remarkably enhanced the membrane's antifouling property that subsequently improved its filtration performance, which is in agreement with the results of this study that combination of UV irradiation followed by PVA coating can further improve the performance of nanohybrid PSf/GO-SiO_2 membrane.

After 8 h of treatment, the pollutant removal ability of several prepared membranes was also measured. Figure 7C shows that the chemical modification of the membrane resulted in higher pollutant removal. The neat PSf membrane removed 28% of TDS, 56% of COD, and 16% of NH_3 with the initial concentrations of 335.78, 242.55, and 175.19 mg/L, respectively. Incorporating GO/SiO_2 nanoparticles into the membrane attained 34% of TDS removal, 75% of COD removal, and 68% of NH_3 removal. This indicates that GO/SiO_2 nanoparticles played roles not only in permeate flux but also in pollutant rejection. Integrating UV irradiation and PVA coating on the PSf/GO-SiO_2 membrane further attained 85% of TDS removal, 81% of COD removal, and 84% of NH_3 removal. Therefore, incorporating GO/SiO_2 nanoparticles with UV irradiation and PVA coating on the PSf membrane significantly improved the physicochemical properties, flux performance, and pollutant rejection ability. This suggests that this technique was effective for the treatment of natural rubber-laden wastewater.

3.8 Cycle test, resistance during filtration, and antifouling performance evaluations

Table 3 summarizes the resistances during filtration on the membrane that was calculated based on intrinsic resistance (R_m), fouling resistance (R_f), and total resistance (R_T). Based on Table 3, it can be seen that the PSf/GO-SiO_2—UV/PVA membrane has the lowest all of the three resistance parameters than the other membranes. This is explainable due to its higher porosity, higher hydrophilicity, and water uptake than those of the other membranes. The addition of GO-SiO_2 nanoparticles as the filler improved membrane porosity, which led to a higher membrane permeate flux. The combined UV irradiation and cross-linked PVA coating treatment to the nanohybrid membrane also enlarged membrane porosity to become larger, stabilized them and reduced the membrane fouling resistance. The presence of excessive solid nanoparticles in the PSf membrane adsorbed on the membrane pores triggered the clogging of the membrane pores as a foulant (Guo et al., 2020; Gupta and Chellam, 2020). Therefore, the unmodified membranes exhibited higher rejection, and lower water permeate flux than the modified membranes. The cross-linked PVA coating on the membrane increased the hydrophilicity and formed a smoother membrane surface. The membrane coatings using PVA enhanced the hydrophilicity of the membrane, subsequently increasing membrane permeability, and reducing the fouling tendency. Consequently, such an increase

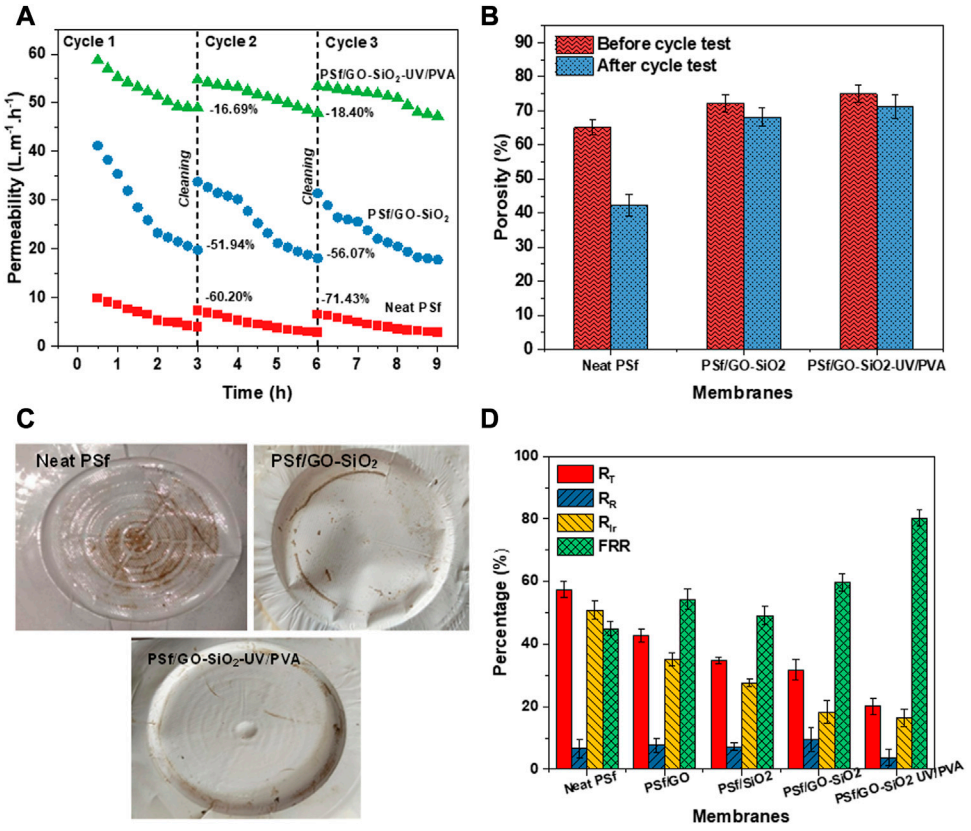

FIGURE 8
(A) The result of three consecutive filtration cycles on the fabricated membranes, **(B)** Membrane porosity analysis of before and after cycle test, **(C)** Images of tested membranes, i.e., neat PSf, PSf/GO-SiO_2, and PSf/GO-SiO_2-UV/PVA after cycle test, and **(D)** The calculation results of fouling resistances, i.e., total resistance (R_T), reversible resistance (R_R), irreversible resistance (R_{Ir}), and flux recovery performance (FRR).

in membrane surface hydrophilicity makes the membrane to be more resistant to fouling.

The cycle test on neat PSf, PSf/GO-SiO_2, and PSf/GO-SiO_2-UV/PVA membranes was evaluated to understand the durability of the membranes upon repetitive usage. The cycle test results are depicted in Figure 8A. It can be observed that all the membranes experienced a gradual flux reduction during the filtration test and got increased in flux after the cleaning process. The neat PSf membrane experienced flux reductions of 60.20% at the end of the first cycle and 71.43% at the second cycle. While the PSf/GO-SiO_2 membrane has slightly better durability and experienced flux reductions of 51.94% and 56.07%. Interestingly, the surface modification using UV exposure and PVA coating on the membrane successfully improved the filtration durability of the membrane, which only has flux reductions of 16.69% at the end of the first cycle and 18.40% at the end of the second cycle. To further understand the root problems that caused the flux reduction on the membranes, a porosity analysis was carried out. Figure 8B presents the membranes' porosities before and after the cycle test. It can be seen that the neat PSf experienced the worst porosity reduction, indicating that the root problem in flux reduction of neat PSf is pore blocking by foulants. Incorporating GO-SiO_2 nanoparticles and subsequent UV irradiation and PVA coating treatments attributed the membrane with high durability to prevent the pore blocking on the membrane and resulting in just a slight reduction in the porosity. Figure 8C shows the image of the neat PSf, PSf/GO-SiO_2, and PSf/GO-SiO_2-UV/PVA membranes after going through the three consecutive cycles test. The dirt on the surface of the membrane shows the existence of foulants. Neat PSf membrane clearly has the worst fouling problem, and the PSf/GO-SiO_2-UV/PVA seems to have the antifouling ability. It is explainable that the combination of GO-SiO_2 nanoparticles incorporation, UV exposure, and PVA coating treatment significantly enhanced the antifouling performance of the membrane.

In addition, the antifouling potential evaluation of the fabricated membrane was carried out. It was measured by calculating the ratios of irreversible fouling (R_{Ir}), reversible fouling (R_R), total fouling (R_T), and flux recovery ratio performance (FRR), as the results are depicted in Figure 8D. Based on the results, it can be found that the neat PSf membrane experienced the highest fouling ratios and lowest FRR. Along with the addition of nanoparticles, i.e., GO, SiO_2, and GO-SiO_2, the fouling ratios gradually decreased. At the same time, the reduction in fouling ratios was further achieved by applying UV exposure and PVA coating. The neat PSf experienced about 56%, 50%, and 6% on R_T, R_{Ir}, and R_R, respectively, while the PSf/GO-

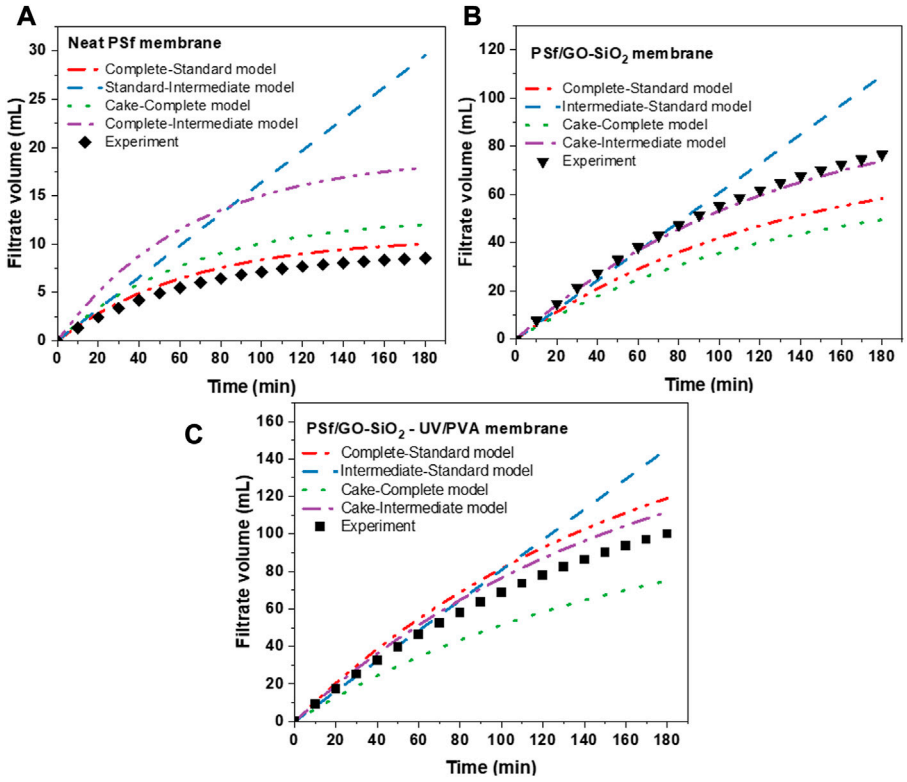

FIGURE 9
Profiles of filtrate volumes to time experimental data compared to complete-standard, intermediate-standard, cake-complete, and cake-intermediate fouling models for: **(A)** neat PSf, **(B)** PSf/GO-SiO_2, and **(C)** PSf/GO-SiO_2—UV/PVA membrane.

SiO_2-UV/PVA membrane just experienced 21%, 19%, and 2% on R_T, R_{Ir}, and R_R, respectively. These findings strengthen the evidence for identifying the root problem that caused the fouling. Moreover; Figure 8D also shows that the flux recovery ratio (FRR) value of the neat PSf membrane was approximately 45%. This value increased to 83% as a result of modification processes, which indicated the improved antifouling characteristic of the modified nanohybrid membranes. The flux recovery ratio of the PSf/GO-SiO_2 membrane without UV irradiation was as low as 59%. This suggests a poor antifouling characteristic, as compared to the PSf GO/SiO_2 —UV/PVA membrane. The PSf nanohybrid membrane with UV irradiation and PVA coating possessed the largest FRR value. The FRR value and lower total fouling ratio values after chemical modification indicated a better antifouling characteristic on the membrane (Younas et al., 2019). This result is in agreement with the reported work by Zheng et al. (2022), who concluded that a novel Cu-BTC@PVA/PVDF membrane is superior to cope with fouling problems due to the presence of hydration layer, slip effect, and electrostatic repulsion from PVA incorporation. So that the membrane can promote a stable flux performance for up to 48 h (Zheng et al., 2022). The cross-linked PVA coating reduced fouling formation on the membrane surface by reducing the adsorptive interactions between the foulant molecules and the membrane surface by enhancing membrane surface hydrophilicity. This implies that the modification of the PSf/GO-SiO_2 membrane with PVA coating on the membrane surface enhanced the antifouling property of the polymeric membrane.

3.9 Evaluation of the fouling mechanisms using combined models

Four combined models were used to evaluate the main fouling type for constant pressure filtration using neat PSf, PSf/GO-SiO_2, and PSf/GO-SiO_2—UV/PVA membranes. The filtrate volume was measured as a function of time and then the experimental data trends were fitted and compared with the tested fouling models. Figure 9 shows the plots of fouling models against experimental data for the three membranes. It can be visually observed that the neat PSf membrane filtrate profile follows the complete-standard models. Meanwhile, the other two membranes follow the pattern of the cake-intermediate model. Further, to confirm the validity of curve fitting and the selection of the best model, the sum of squared residual (SSR) is calculated. In statistics, the Sum of Squared Residuals (SSR), also known as the residual sum of squares or the sum of squared estimate of errors (SSE), is a measure of the amount of variance in a data set that is not explained by a statistical model (Silva et al., 2013).

TABLE 4 Sum of squared residuals (SSR) of applied models for neat PSf, PSf/GO-SiO_2, and PSf/GO-SiO_2—UV/PVA membranes.

Model	Sum of squared residuals (SSR)		
	Neat PSf	PSf/GO-SiO_2	PSf/GO-SiO_2—UV/PVA
Complete-Standard	23.70*	2,944.53	3,945.21
Standard-Intermediate	2,336.13	3,706.87	8058.91
Cake-Complete	131.08	6,415.44	5,213.80
Cake-Intermediate	953.41	66.78*	1,115.49*

*least sum squared residuals = the best fitted model.

TABLE 5 Fitted parameters of applied models for neat PSf, PSf/GO-SiO_2, and PSf/GO-SiO_2—UV/PVA membranes.

Model	Fitted parameters		
	Neat PSf	PSf/GO-SiO_2	PSf/GO-SiO_2—UV/PVA
Complete-Standard	$K_b = 2.56 \times 10^{-4}$ s^{-1}	$K_b = 1.32 \times 10^{-4}$ s^{-1}	$K_b = 1.02 \times 10^{-4}$ s^{-1}
	$K_s = 6.88$ m^{-1}	$K_s = 5.74$ m^{-1}	$K_s = 4.83$ m^{-1}
Standard-Intermediate	$K_i = 3.01$ m^{-1}	$K_i = 2.81$ m^{-1}	$K_i = 2.26$ m^{-1}
	$K_s = 6.88$ m^{-1}	$K_s = 5.74$ m^{-1}	$K_s = 4.83$ m^{-1}
Cake-Complete	$K_b = 2.56 \times 10^{-4}$ s^{-1}	$K_b = 1.32 \times 10^{-4}$ s^{-1}	$K_b = 1.02 \times 10^{-4}$ s^{-1}
	$K_c = 1.30 \times 10^{4}$ sm^{-2}	$K_c = 1.15 \times 10^{3}$ sm^{-2}	$K_c = 9.85 \times 10^{1}$ sm^{-2}
Cake-Intermediate	$K_c = 1.30 \times 10^{4}$ sm^{-2}	$K_c = 1.15 \times 10^{4}$ sm^{-2}	$K_c = 9.85 \times 10^{1}$ sm^{-2}
	$K_i = 3.01$ m^{-1}	$K_i = 2.81$ m^{-1}	$K_i = 2.26$ m^{-1}

Essentially, it measures the difference between the predicted values of a model and the actual values observed in the data. The SSR is calculated by taking the squared difference between each predicted value and its corresponding actual value, and then summing these squared differences over the entire data set. The resulting value represents the overall amount of unexplained variation in the data and can be used to evaluate the goodness-of-fit of a statistical model (Li Z. et al., 2021). A lower SSR indicates a better fit of the model to the data, while a higher SSR suggests that the model may not be capturing all of the underlying patterns in the data (Silva et al., 2013). Therefore, minimizing the SSR is a common goal in statistical modeling and regression analysis. Table 4 summarized the SSR values of the applied models for each membrane. It is found that the least sum of squared residuals is the complete-standard model (SSR = 23.70) for the neat PSf membrane, and cake-intermediate model for PSf/GO-SiO_2 (SSR = 66.78) and PSf/GO-SiO_2—UV/PVA (SSR = 1115.9) membranes.

Moreover, the fitted parameters of the applied models are assessed, as the results are listed in Table 5. It is found that K_b and K_s control the filtrate volume of the neat PSf membrane. It is also explainable that the combined complete and standard blocking is the main mechanism, which controls the fouling on the neat PSf membrane. Under this mechanism, the membrane pores are constricted by solid substances that accumulated uniformly on the membrane pores (Ho and Zydney, 2000). As a result, compact pore plugging occurred, thus resulting in a rapid reduction of permeate flow. It can be happened due to the poor surface hydrophilicity of the neat PSf membrane, which promoted ease of pollutant attachments. Apart from that, the PSf/GO-SiO_2 possessed the cake-intermediate model with K_c and K_i as the main contributors controlling permeate flow of the membrane. It can be described that the GO-SiO_2 addition changed the surface properties of the membrane, thus resulting in an improved antifouling ability. Similarly, the modified membrane PSF/GO-SiO_2—UV/PVA followed the cake-intermediate model. The fouling mechanisms of this model are controlled by caking and intermediate pore blocking. Compared to the neat PSf, it can be seen that the modified membranes can maintain the filtrate flow better. It can be promoted by the reduction of pore-blocking formation on the membrane surface (Kim et al., 2013). The hydrophilic membrane surface using PVA coating can perform a repulsion force against the hydrophobic particulates and prevent pore-clogging (Mahamadou et al., 2019). Therefore, it is noteworthy that the addition of GO-SiO_2 nanoparticles and sequential UV/PVA treatment on the membrane surface can be helpful in preventing pore-blocking formation on the membrane surface.

3.10 Comparison to the other methods in the literature

Table 6 summarizes recent methods that have been investigated in the treatment of industrial rubber wastewater. Some conventional methods including coagulation-flocculation,

TABLE 6 Comparison of other treatment methods of rubber wastewater in the literature.

Method	Operating condition	Key findings	Ref
Anaerobic digestion	Temperature = 26–32°C, Reactor volume = 5.8 L, Sponge volume = 3.9 L, Feed organic rate = 1 kg COD/m^3 day, N_2 input rate = 0.57 kg/m^3 day	COD removal = 64.2%	Watari et al. (2017a)
		TN removal = 55.3%	
Anaerobic digestion	Reactor volume = 0.8 L, Flow rate = 1.3–4 m^3/day, Process duration = 13.9–63.4 h, Organic feed rate = 0.7–3.1 kg/m^3 d	COD removal = 55.6%	Watari et al. (2017b)
		BOD removal = 77.8%	
Coagulation and anaerobic	Coagulation: $CaCl_2$ concentration = 0–7710 mg/L, pH = 4.8, 7, and 10.3 Anaerobic: Temperature = 35°C, VS. = 3,000 mg/L, Reactor volume = 2.8, pH = 7.5	COD removal = 84%	Rudra Paul et al. (2022)
		BOD removal = 91%	
		CH_4 recovery = 1.47 Nm^3/m^3 day	
Coagulation - flocculation and anaerobic	Coagulation-flocculation: $Al_2(SO_4)_3$ conc. = 0–1,000 mg/L, pH = 4–8 Anaerobic: Reactor volume = 2L, Inoculum concentration = 10 wt%	COD removal = 64.38%	Nguyen et al. (2018)
		BOD removal = 71.43%	
		TSS removal = 65.96%	
		N removal = 54.12%	
		P removal = 79.86%	
		Cumulative H_2 = 221 mL/L (max)	
Fenton and adsorption	Fenton: Fenton chemical = $FeSO_4$, pH = 3.5, Fe^{2+}: peroxide molar ratio = 1:150–1:250 Adsorption: Adsorbent = activated carbon, Bed height = 20 cm	The highest removal of COD of 95% was achieved by applying Fenton molar ratio of 1:250	Emilia Agustina et al. (2017)
Microbial fuel cell (MFC)	Working volume = 2.5–4 L Ionic membrane = Nafion 212 (proton exchange membrane), Membrane diameter = 4 cm, Electrodes = graphite	COD removal = 72.4%	Nookwam et al. (2022)
		N removal = 40.5%	
		P removal = 24.4%	
		Max. power density = 55.43 W/m^3	
Membrane ultrafiltration	Polymer = PAN, Pore size = 12–102 nm, Surface area = 72.25 cm^2, Porosity = 9%–25%, Pressure = 1 bar, No filler and other modifications	COD removal = 38%	Nazri et al. (2015)
		TOC removal = 32%	
		TDS removal = 11%	
		Conductivity removal = 8%	
		Proteins removal = 70%	
		Color removal = 97%	
		Turbidity removal = 99%	
		Flux recovery = 84%	
Photocatalytic membrane	Polymer = PSf, Filler = ZnO-MnO_2@SiO_2 composite, Porosity = 72.31%, Pore size = 42.76 nm, Surface area = 12.56 cm^2, UV lamp power = 30 W, Pressure = 5 bar	TDS removal = 73.26%	Kusworo et al. (2023)
		COD removal = 78.92%	
		NH_3-N removal = 75.69%	
		Permeate flux = 27.31 L/m^2h	
		Flux recovery = 88%	
Modified ultrafiltration membrane	Polymer = PSf, Filler = GO-SiO_2, Surface modification = PVA assisted UV irradiation, PVA concentration = 0.5 wt%, UV irradiation duration = 3 min, Porosity = 75%, Pore size = 36 nm, Surface area = 12.56 cm^2, Pressure = 5 bar	TDS removal = 85%	[This study]
		COD removal = 84%	
		Permeate flux = 50.32 L/m^2h	
		Flux recovery = 83%	
		Able to tackle severe fouling problem	

adsorption, and anaerobic digestions have been studied along with promising results. Modern methods have been also employed in treating this kind of wastewater such as microbial fuel cell (MFC), ultrafiltration, and photocatalytic membrane. In comparison, it is clearly observed that conventional methods required more chemicals and equipment than modern methods. Particularly, in membrane technology, it is required the least chemicals to process the wastewater, as well as it can provide high pollutant rejection performance. One of the major benefits of membrane technology is its ability to remove contaminants with high efficiency and selectivity. Ultrafiltration, for example, can be very effective in removing colloids and other small particles from wastewater (Lu et al., 2021). Moreover, membrane technology allows for a more continuous and automated process, reducing the need for manual intervention and minimizing the risk of human error. Membrane technology has also become a key technology for industrial separations, and it is expected to play an even more important role in future sustainable production (Shenvi et al., 2015). The future prospects of membrane technology are promising, and there are ongoing efforts to develop new and improved membrane materials and processes. One of the most significant areas of research is the development of alternative membrane materials, such as graphemic derivatives and carbon nanotubes, which have unique properties that make them ideal for certain separations, as demonstrated in this work. Additionally, researchers are working to improve membrane processes, such as membrane bioreactors and photocatalytic membranes, to make them more efficient and cost-effective. Overall, this study contributed to expanding the insights about an effective method in rubber wastewater treatment by applying the surface and composite modification using UV-assisted PVA coating along with GO-SiO_2 addition in PSf membrane, which resulted in exquisite separation performance.

4 Conclusion

This study has demonstrated that the performance of the modified PSf/GO-SiO_2 nanohybrid membrane with UV irradiation and cross-linked PVA coating has been significantly better than that of the unmodified membrane. It is found that combined UV irradiation and cross-linked PVA coating provided an excellent antifouling characteristic of the membrane by enhancing membrane surface hydrophilicity that significantly decreased from 67.75° for the PSf/GO-SiO_2 to 35.17° for the modified PSf/GO-SiO_2 by UV irradiation and PVA coating. It also improved the water uptake ability and membrane affinity towards water molecules. The PSf–GO 1 wt%—SiO_2 0.5 wt % −3 min UV–PVA 0.5 wt% membrane exhibited the highest and the most stable flux. The UV irradiation and cross-linked PVA coating to the PSf/GO-SiO_2 nanohybrid membrane improved the pseudo-steady state permeate water flux by 60.15% from 20.05 to 50.32 L/m^2hr and maintained the permeate flux up to 82.33%. About 85% of total dissolved solids (TDS), 81% of chemical oxygen demand (COD), and 84% of ammonia compound (NH_3) with initial concentrations of 335.76, 242.55, 175.19 mg/L, respectively, could be removed after 8 h of membrane treatment. The cycle test results showed that PSf/GO-SiO_2-UV/PVA experienced a flux reduction of only 16.69% at the end of the first cycle and 18.40% at the end of the second cycle, with a flux recovery ratio of 83%. The cross-linked PVA coating reduced fouling formation on the membrane surface by reducing the adsorptive interactions between the foulant molecules and the membrane surface by enhancing membrane surface hydrophilicity. Additionally, the addition of GO-SiO_2 nanoparticles and UV/PVA coating treatment on the membrane surface successfully improved the membrane's fouling mechanism from pore blockage into a cake filtration mechanism, which signifies the ability of the membrane to tackle the severe fouling problem. This implies that incorporating GO/SiO_2 nanoparticles with UV irradiation and PVA coating on the PSf membrane substantially enhanced the physicochemical properties, antifouling properties, flux performance, and pollutant rejection ability. Overall, the results of this study provide insightful ideas for future applications of membranes with prominent antifouling properties for not only natural rubber-laden wastewater but also other wastewater with high organic pollutant contents.

Data availability statement

The original contributions presented in the study are included in the article/Supplementary Material, further inquiries can be directed to the corresponding author.

Author contributions

TK: conceptualization, methodology, resources, writing–original draft. AK: supervision and validation. NA: formal analysis and validation. FL: investigation and collecting data. AW: investigation and formal analysis. AV: resources and writing-review and editing. FD: formal analysis, data curation, visualization, writing-review and editing.

Funding

This paper has been supported by the RUDN University Strategic Academic Leadership Program (recipient AV). This research is fully funded by Diponegoro University World-Class Research Grant (WCR-UNDIP) No. 118-31/UN7.6.1/PP/2021.

Acknowledgments

The authors fully acknowledged Institute for Research and Community Services (LPPM), Universitas Diponegoro, for the approved fund, which makes this critical research viable and effective. The author would also thank the PTPN VII in Bengkulu, Indonesia, for the sample of natural rubber-laden wastewater that was used in this study. AV gratefully acknowledges that this paper has been supported by the RUDN University Strategic Academic Leadership Program (for AV).

Conflict of interest

The authors declare that the research was conducted in the absence of any commercial or financial relationships that could be construed as a potential conflict of interest.

Publisher's note

All claims expressed in this article are solely those of the authors and do not necessarily represent those of their affiliated organizations, or those of the publisher, the editors and the reviewers. Any product that may be evaluated in this article, or claim that may be made by its manufacturer, is not guaranteed or endorsed by the publisher.

Supplementary material

The Supplementary Material for this article can be found online at: https://www.frontiersin.org/articles/10.3389/fenvs.2023.1175957/full#supplementary-material

References

Alkhouzaam, A., and Qiblawey, H. (2021). Functional GO-based membranes for water treatment and desalination: Fabrication methods, performance and advantages. A review. *Chemosphere* 274, 129853. doi:10.1016/J.CHEMOSPHERE.2021.129853

Álvarez Bayona, M. A., Maturana Córdoba, A., Gallardo Amaya, R. J., and Muñoz Acevedo, A. (2022). Occurrence of glyphosate in surface and drinking water sources in Cúcuta, Norte de Santander, and its removal using membrane technology. *Front. Environ. Sci.* 10. doi:10.3389/fenvs.2022.941836

Arifeen, W. U., Kim, M., Choi, J., Yoo, K., Kurniawan, R., and Ko, T. J. (2019). Optimization of porosity and tensile strength of electrospun polyacrylonitrile nanofibrous membranes. *Mater Chem. Phys.* 229, 310–318. doi:10.1016/J.MATCHEMPHYS.2019.03.020

Bai, L., Wu, H., Ding, J., Ding, A., Zhang, X., Ren, N., et al. (2020). Cellulose nanocrystal-blended polyethersulfone membranes for enhanced removal of natural organic matter and alleviation of membrane fouling. *Chem. Eng. J.* 382, 122919. doi:10.1016/j.cej.2019.122919

Bakry, A. M., Alamier, W. M., Salama, R. S., Samy El-Shall, M., and Awad, F. S. (2022). Remediation of water containing phosphate using ceria nanoparticles decorated partially reduced graphene oxide (CeO2-PRGO) composite. *Surfaces Interfaces* 31, 102006. doi:10.1016/j.surfin.2022.102006

Baroña, G. N. B., Choi, M., and Jung, B. (2012). High permeate flux of PVA/PSf thin film composite nanofiltration membrane with aluminosilicate single-walled nanotubes. *J. Colloid Interface Sci.* 386, 189–197. doi:10.1016/J.JCIS.2012.07.049

Bell, E. A., Poynor, T. E., Newhart, K. B., Regnery, J., Coday, B. D., and Cath, T. Y. (2017). Produced water treatment using forward osmosis membranes: Evaluation of extended-time performance and fouling. *J. Memb. Sci.* 525, 77–88. doi:10.1016/j.memsci.2016.10.032

Bolton, G., LaCasse, D., and Kuriyel, R. (2006). Combined models of membrane fouling: Development and application to microfiltration and ultrafiltration of biological fluids. *J. Memb. Sci.* 277, 75–84. doi:10.1016/j.memsci.2004.12.053

Chai, P. v., Law, J. Y., Mahmoudi, E., and Mohammad, A. W. (2020). Development of iron oxide decorated graphene oxide (Fe3O4/GO) PSf mixed-matrix membrane for enhanced antifouling behavior. *J. Water Process Eng.* 38, 101673. doi:10.1016/J.JWPE.2020.101673

Chaumien, E., Boda, R., and Boutarin, L. (2012). Reuse of waste water to make drinking water by using RO membranes technology: Technical feasibility and European regulation. *Procedia Eng.* 44, 1726. doi:10.1016/j.proeng.2012.08.924

Chiao, Y.-H., Chen, S.-T., Yap Ang, M. B. M., Patra, T., Castilla-Casadiego, D. A., Fan, R., et al. (2020). High-performance polyacrylic acid-grafted PVDF nanofiltration membrane with good antifouling property for the textile industry. *Polym. (Basel)* 12, 2443. doi:10.3390/polym12112443

Dalanta, F., Kusworo, T. D., and Aryanti, N. (2022). Synthesis, characterization, and performance evaluation of UV light-driven Co-TiO2@SiO2 based photocatalytic nanohybrid polysulfone membrane for effective treatment of petroleum refinery wastewater. *Appl. Catal. B* 316, 121576. doi:10.1016/j.apcatb.2022.121576

Das, T. K., Bhawal, P., Ganguly, S., Mondal, S., and Das, N. Ch. (2018). A facile green synthesis of amino acid boosted Ag decorated reduced graphene oxide nanocomposites and its catalytic activity towards 4-nitrophenol reduction. *Surfaces Interfaces* 13, 79–91. doi:10.1016/j.surfin.2018.08.004

Dehban, A., Kargari, A., and Ashtiani, F. Z. (2020). Preparation and optimization of antifouling PPSU/PES/SiO2 nanocomposite ultrafiltration membranes by VIPS-NIPS technique. *J. Indust. Eng. Chem.* 88, 292–311. doi:10.1016/J.JIEC.2020.04.028

Dmitrenko, M., Kuzminova, A., Zolotarev, A., Liamin, V., Plisko, T., Burts, K., et al. (2021). Novel high flux poly(m-phenylene isophtalamide)/TiO2 membranes for ultrafiltration with enhanced antifouling performance. *Polym. (Basel)* 13, 2804. doi:10.3390/polym13162804

Ebrahimi, F., Nabavi, S. R., and Omrani, A. (2022). Fabrication of hydrophilic special sandwich structure of PAN/GO/SiO2 electrospun membrane decorated with SiO2 nanoparticles for oil/water separation. *J. Water Process Eng.* 48, 102926. doi:10.1016/j.jwpe.2022.102926

Emilia Agustina, T., Jefri Sirait, E., and Silalahi, H. (2017). Treatment of rubber industry wastewater by using fenton reagent and activated carbon. *J. Teknol.* 79. doi:10.11113/jt.v79.11872

Evdochenko, E., Kamp, J., Dunkel, R., Nikonenko, V. v., and Wessling, M. (2021). Charge distribution in polyelectrolyte multilayer nanofiltration membranes affects ion separation and scaling propensity. *J. Memb. Sci.* 636, 119533. doi:10.1016/J.MEMSCI.2021.119533

Fan, G., Chen, C., Chen, X., Li, Z., Bao, S., Luo, J., et al. (2021). Enhancing the antifouling and rejection properties of PVDF membrane by Ag3PO4-GO modification. *Sci. Total Environ.* 801, 149611. doi:10.1016/J.SCITOTENV.2021.149611

Feng, L., Gao, Y., Xu, Y., Dan, H., Qi, Y., Wang, S., et al. (2021). A dual-functional layer modified GO@SiO2 membrane with excellent anti-fouling performance for continuous separation of oil-in-water emulsion. *J. Hazard Mater* 420, 126681. doi:10.1016/J.JHAZMAT.2021.126681

Ganesh, B. M., Isloor, A. M., and Ismail, A. F. (2013). Enhanced hydrophilicity and salt rejection study of graphene oxide-polysulfone mixed matrix membrane. *Desalination* 313, 199–207. doi:10.1016/J.DESAL.2012.11.037

Ganguly, S., Mondal, S., Das, P., Bhawal, P., Das, T. K., Ghosh, S., et al. (2019). An insight into the physico-mechanical signatures of silylated graphene oxide in poly(ethylene methyl acrylate) copolymeric thermoplastic matrix. *Macromol. Res.* 27, 268–281. doi:10.1007/s13233-019-7039-y

Gao, Y., Yan, N., Jiang, C., Xu, C., Yu, S., Liang, P., et al. (2020). Filtration-enhanced highly efficient photocatalytic degradation with a novel electrospun rGO@TiO2 nanofibrous membrane: Implication for improving photocatalytic efficiency. *Appl. Catal. B* 268, 118737. doi:10.1016/j.apcatb.2020.118737

Guo, Y., Li, T., Xiao, K., Wang, X., and Xie, Y. F. (2020). Key foulants and their interactive effect in organic fouling of nanofiltration membranes. *J. Memb. Sci.* 610, 118252. doi:10.1016/j.memsci.2020.118252

Gupta, K., and Chellam, S. (2020). Contributions of surface and pore deposition to (ir) reversible fouling during constant flux microfiltration of secondary municipal wastewater effluent. *J. Memb. Sci.* 610, 118231. doi:10.1016/j.memsci.2020.118231

Habashi, N., Mehrdadi, N., Mennerich, A., Alighardashi, A., and Torabian, A. (2016). Hydrodynamic cavitation as a novel approach for pretreatment of oily wastewater for anaerobic co-digestion with waste activated sludge. *Ultrason. Sonochem* 31, 362–370. doi:10.1016/J.ULTSONCH.2016.01.022

Hashino, M., Katagiri, T., Kubota, N., Ohmukai, Y., Maruyama, T., and Matsuyama, H. (2011). Effect of surface roughness of hollow fiber membranes with gear-shaped structure on membrane fouling by sodium alginate. *J. Memb. Sci.* 366, 389–397. doi:10.1016/j.memsci.2010.10.025

Ho, C.-C., and Zydney, A. L. (2000). A combined pore blockage and cake filtration model for protein fouling during microfiltration. *J. Colloid Interface Sci.* 232, 389–399. doi:10.1006/jcis.2000.7231

Horseman, T., Wang, Z., and Lin, S. (2021). Colloidal interactions between model foulants and engineered surfaces: Interplay between roughness and surface energy. *Chem. Eng. J. Adv.* 8, 100138. doi:10.1016/j.ceja.2021.100138

Hu, D., Luo, K., Ma, H., Min, H., Zhao, Y., Cui, Y., et al. (2020). A sustainability anti-infective pharmaceutical wastewater treatment technology: Multi-stage vertical variable diameter membrane bioreactor with DO online controlling. *Bioresour. Technol.* 311, 123507. doi:10.1016/J.BIORTECH.2020.123507

Jain, M., Majumder, A., Sarathi, P., and Kumar, A. (2020). A review on treatment of petroleum refinery and petrochemical plant wastewater: A special emphasis on constructed wetlands. *J. Environ. Manage* 272, 111057. doi:10.1016/j.jenvman.2020.111057

Kazemi, F., Jafarzadeh, Y., Masoumi, S., and Rostamizadeh, M. (2021). Oil-in-water emulsion separation by PVC membranes embedded with GO-ZnO nanoparticles. *J. Environ. Chem. Eng.* 9, 104992. doi:10.1016/J.JECE.2020.104992

Kim, M., Sankararao, B., Lee, S., and Yoo, C. (2013). Prediction and identification of membrane fouling mechanism in a membrane bioreactor using a combined mechanistic model. *Ind. Eng. Chem. Res.* 52, 17198–17205. doi:10.1021/ie402056r

Kusworo, T. D., Aryanti, N., and Dalanta, F. (2021a). Effects of incorporating ZnO on characteristic, performance, and antifouling potential of PSf membrane for PRW treatment. *IOP Conf. Ser. Mater Sci. Eng.* 1053, 012134. doi:10.1088/1757-899x/1053/1/012134

Kusworo, T. D., Dalanta, F., Aryanti, N., and Othman, N. H. (2021b). Intensifying separation and antifouling performance of PSf membrane incorporated by GO and ZnO nanoparticles for petroleum refinery wastewater treatment. *J. Water Process Eng.* 41, 102030. doi:10.1016/J.JWPE.2021.102030

Kusworo, T. D., Kumoro, A. C., Aryanti, N., Kurniawan, T. A., Dalanta, F., and Alias, N. H. (2023). Photocatalytic polysulfone membrane incorporated by ZnO-MnO2@SiO2 composite under UV light irradiation for the reliable treatment of natural rubber-laden wastewater. *Chem. Eng. J.* 451, 138593. doi:10.1016/j.cej.2022.138593

Li, F., Amenorfenyo, D. K., Zhang, Y., Zhang, N., Li, C., and Huang, X. (2021a). Cultivation of chlorella vulgaris in membrane-treated industrial distillery wastewater: Growth and wastewater treatment. *Front. Environ. Sci.* 9. doi:10.3389/fenvs.2021.770633

Li, Z., Lu, D., and Gao, X. (2021b). Optimization of mixture proportions by statistical experimental design using response surface method - a review. *J. Build. Eng.* 36, 102101. doi:10.1016/j.jobe.2020.102101

Li, S., Bai, L., Luo, X., Ding, J., Li, G., and Liang, H. (2022). A CNT/PVA film supported TFC membranes for improvement of mechanical properties and chemical cleaning stability: A new insight to an alternative to the polymeric support. *J. Memb. Sci.* 658, 120753. doi:10.1016/j.memsci.2022.120753

Liu, X., Zhao, S., Zhang, X., Jia, W., Zou, Z., and Wang, Q. (2020). Application of sodium alginate as a coagulant aid for mitigating membrane fouling induced by humic acid in dead-end ultrafiltration process. *Sep. Purif. Technol.* 253, 117421. doi:10.1016/J.SEPPUR.2020.117421

Liu, Y., Wang, J., Wang, Y., Zhu, H., Xu, X., Liu, T., et al. (2021). High-flux robust PSf-b-PEG nanofiltration membrane for the precise separation of dyes and salts. *Chem. Eng. J.* 405, 127051. doi:10.1016/J.CEJ.2020.127051

Lu, Q., Li, N., and Zhang, X. (2021). Supramolecular recognition PVDF/PVA ultrafiltration membrane for rapid removing aromatic compounds from water. *Chem. Eng. J.* 436, 132889. doi:10.1016/J.CEJ.2021.132889

Mahamadou, B., Benkortbi, O., Hanini, S., and Amrane, A. (2019). Modeling of transitional pore blockage to cake filtration and modified fouling index – dynamical surface phenomena in membrane filtration. *Chem. Eng. Sci.* 193, 298–311. doi:10.1016/j.ces.2018.07.054

Mahdavi, H., Kerachian, M. A., and Abazari, M. (2022). Synergistic effect of GO@SiO2 and GO@ZnO nano-hybrid particles with PVDF-g-PMMA copolymer in high-flux ultrafiltration membrane for oily wastewater treatment and antifouling properties. *J. Industrial Eng. Chem.* 108, 374–388. doi:10.1016/j.jiec.2022.01.016

Martínez, R., Ruiz, M. O., Ramos, C., Cámara, J. M., and Diez, V. (2021). Fouling control of submerged and side-stream membrane bioreactors based on the statistical analysis of mid-term assays. *J. Clean. Prod.* 326, 129336. doi:10.1016/j.jclepro.2021.129336

Medhat Bojnourd, F., and Pakizeh, M. (2018). Preparation and characterization of a PVA/PSf thin film composite membrane after incorporation of PSSMA into a selective layer and its application for pharmaceutical removal. *Sep. Purif. Technol.* 192, 5–14. doi:10.1016/J.SEPPUR.2017.09.054

Motahari, F., and Raisi, A. (2020). UV irradiation-assisted cross-linking of high molecular weight poly (ethylene oxide) with poly (ethylene glycol) diacrylate to prepare CO2 selective membranes. *Polym. Guildf.* 205, 122821. doi:10.1016/j.polymer.2020.122821

Nazri, N. A. M., Lau, W. J., Ismail, A. F., Matsuura, T., Veerasamy, D., and Hilal, N. (2015). Performance of PAN-based membranes with graft copolymers bearing hydrophilic PVA and PAN segments in direct ultrafiltration of natural rubber effluent. *Desalination* 358, 49–60. doi:10.1016/j.desal.2014.12.012

Nguyen, T. A. D., Thi, B. D. N., Le, T. D., and Nguyen, H. L. H. (2018). Biohydrogen fermentation from rubber latex processing wastewater pretreated by aluminium sulphate flocculation. *Int. J. Environ. Waste Manag.* 21, 141. doi:10.1504/IJEWM.2018.10013994

Nguyen, V. H., Tran, Q. B., Nguyen, X. C., Hai, L. T., Ho, T. T. T., Shokouhimehr, M., et al. (2020). Submerged photocatalytic membrane reactor with suspended and immobilized N-doped TiO2 under visible irradiation for diclofenac removal from wastewater. *Process Saf. Environ. Prot.* 142, 229–237. doi:10.1016/J.PSEP.2020.05.041

Nguyen, T. Q., Tung, K. L., Lin, Y. L., Dong, C. di, Chen, C. W., and Wu, C. H. (2021). Modifying thin-film composite forward osmosis membranes using various SiO2 nanoparticles for aquaculture wastewater recovery. *Chemosphere* 281, 130796. doi:10.1016/J.CHEMOSPHERE.2021.130796

Nookwam, K., Cheirsilp, B., Maneechote, W., Boonsawang, P., and Sukkasem, C. (2022). Microbial fuel cells with Photosynthetic-Cathodic chamber in vertical cascade for integrated Bioelectricity, biodiesel feedstock production and wastewater treatment. *Bioresour. Technol.* 346, 126559. doi:10.1016/j.biortech.2021.126559

Park, J., Gaines, K. E., Jheng, L.-C., Riffle, J. S., Mecham, S. J., McGrath, J. E., et al. (2020). Characterization and gas transport properties of UV-irradiated polydimethylsiloxane (PDMS)-containing polyimide copolymer membranes. *Polym. Guildf.* 210, 122966. doi:10.1016/j.polymer.2020.122966

Rambabu, K., Bharath, G., Arangadi, A. F., Velu, S., Banat, F., and Show, P. L. (2020). ZrO2 incorporated polysulfone anion exchange membranes for fuel cell applications. *Int. J. Hydrogen Energy* 45, 29668–29680. doi:10.1016/J.IJHYDENE.2020.08.175

Rao, A. S., Rashmi, K. R., Manjunatha, D. V., Jayarama, A., Prabhu, S., and Pinto, R. (2019). Pore size tuning of Nafion membranes by UV irradiation for enhanced proton conductivity for fuel cell applications. *Int. J. Hydrogen Energy* 44, 23762–23774. doi:10.1016/j.ijhydene.2019.07.084

Rudra Paul, S., Das, R., and Debnath, A. (2022). Sequential coagulation/flocculation and sonolytic oxidation using persulfate and hydrogen peroxide for real rubber processing industry wastewater treatment: Kinetic modelling and treatment cost analysis. *Mater Today Proc.* 77, 247–253. doi:10.1016/j.matpr.2022.11.270

Scalia, A., Bella, F., Lamberti, A., Gerbaldi, C., and Tresso, E. (2019). Innovative multipolymer electrolyte membrane designed by oxygen inhibited UV-crosslinking enables solid-state in plane integration of energy conversion and storage devices. *Energy* 166, 789–795. doi:10.1016/j.energy.2018.10.162

Shakak, M., Rezaee, R., Maleki, A., Jafari, A., Safari, M., Shahmoradi, B., et al. (2020). Synthesis and characterization of nanocomposite ultrafiltration membrane (PSF/PVP/SiO2) and performance evaluation for the removal of amoxicillin from aqueous solutions. *Environ. Technol. Innov.* 17, 100529. doi:10.1016/J.ETI.2019.100529

Sharma, N., Lavania, M., and Lal, B. (2020). Development and demonstration of membrane to control potential pathogen (Legionella sp.) associated with cooling towers. *Front. Environ. Sci.* 8. doi:10.3389/fenvs.2020.570904

Shenvi, S. S., Isloor, A. M., and Ismail, A. F. (2015). A review on RO membrane technology: Developments and challenges. *Desalination* 368, 10–26. doi:10.1016/j.desal.2014.12.042

Silva, L. J., Panzera, T. H., Velloso, V. R., Rubio, J. C. C., Christoforo, A. L., and Scarpa, F. (2013). Statistical design of polymeric composites reinforced with banana fibres and silica microparticles. *J. Compos Mater* 47, 1199–1210. doi:10.1177/0021998312446499

Su, Q. W., Lu, H., Zhang, J. Y., and Zhang, L. Z. (2019). Fabrication and analysis of a highly hydrophobic and permeable block GO-PVP/PVDF membrane for membrane humidification-dehumidification desalination. *J. Memb. Sci.* 582, 367–380. doi:10.1016/J.MEMSCI.2019.04.023

Sugumar, M., Kugarajah, V., and Dharmalingam, S. (2022). Optimization of operational factors using statistical design and analysis of nanofiller incorporated polymer electrolyte membrane towards performance enhancement of microbial fuel cell. *Process Saf. Environ. Prot.* 158, 474–485. doi:10.1016/j.psep.2021.12.018

Tran, M. L., Fu, C. C., Chiang, L. Y., Hsieh, C. te, Liu, S. H., and Juang, R. S. (2020). Immobilization of TiO2 and TiO2-GO hybrids onto the surface of acrylic acid-grafted polymeric membranes for pollutant removal: Analysis of photocatalytic activity. *J. Environ. Chem. Eng.* 8, 104422. doi:10.1016/J.JECE.2020.104422

Vatanpour, V., Nekouhi, G. N., and Esmaeili, M. (2020). Preparation, characterization and performance evaluation of ZnO deposited polyethylene ultrafiltration membranes for dye and protein separation. *J. Taiwan Inst. Chem. Eng.* 114, 153–167. doi:10.1016/J.JTICE.2020.09.008

Vaysizadeh, A., Zinatizadeh, A. A., and Zinadini, S. (2021). Fouling mitigation and enhanced dye rejection in UF and NF membranes via layer-by-layer (LBL) assembly and altering PVP percentage as pore former. *Environ. Technol. Innov.* 23, 101698. doi:10.1016/J.ETI.2021.101698

Vazquez-Jaime, M., Arcibar-Orozco, J. A., Damian-Ascencio, C. E., Saldaña-Robles, A. L., Martínez-Rosales, M., Saldaña-Robles, A., et al. (2020). Effective removal of arsenic from an aqueous solution by ferrihydrite/goethite graphene oxide composites using the modified Hummers method. *J. Environ. Chem. Eng.* 8, 104416. doi:10.1016/J.JECE.2020.104416

Vinardell, S., Astals, S., Peces, M., Cardete, M. A., Fernández, I., Mata-Alvarez, J., et al. (2020). Advances in anaerobic membrane bioreactor technology for municipal wastewater treatment: A 2020 updated review. *Renew. Sustain. Energy Rev.* 130, 109936. doi:10.1016/J.RSER.2020.109936

Wang, C., Song, X., Liu, Y., and Zhang, C. (2021). PVC-g-PVP amphiphilic polymer synthesis by ATRP and its membrane separation performance for silicone-containing wastewater. *Polym. Guildf.* 229, 123965. doi:10.1016/J.POLYMER.2021.123965

Wanke, D., da Silva, A., and Costa, C. (2021). Modification of PVDF hydrophobic microfiltration membrane with a layer of electrospun fibers of PVP-co-PMMA: Increased fouling resistance. *Chem. Eng. Res. Des.* 171, 268–276. doi:10.1016/J.CHERD.2021.05.004

Watari, T., Cuong Mai, T., Tanikawa, D., Hirakata, Y., Hatamoto, M., Syutsubo, K., et al. (2017a). Development of downflow hanging sponge (DHS) reactor as post

treatment of existing combined anaerobic tank treating natural rubber processing wastewater. *Water Sci. Technol.* 75, 57–68. doi:10.2166/wst.2016.487

Watari, T., Mai, T. C., Tanikawa, D., Hirakata, Y., Hatamoto, M., Syutsubo, K., et al. (2017b). Performance evaluation of the pilot scale upflow anaerobic sludge blanket – downflow hanging sponge system for natural rubber processing wastewater treatment in South Vietnam. *Bioresour. Technol.* 237, 204–212. doi:10.1016/j.biortech.2017.02.058

Wu, H., Tang, B., and Wu, P. (2014). Development of novel SiO2–GO nanohybrid/polysulfone membrane with enhanced performance. *J. Memb. Sci.* 451, 94–102. doi:10.1016/J.MEMSCI.2013.09.018

Younas, H., Zhou, Y., Li, X., Li, X., Sun, Q., Cui, Z., et al. (2019). Fabrication of high flux and fouling resistant membrane: A unique hydrophilic blend of polyvinylidene fluoride/polyethylene glycol/polymethyl methacrylate. *Polym. Guildf.* 179, 121593. doi:10.1016/J.POLYMER.2019.121593

Younes, Y. A., Kospa, D. A., Salama, R. S., Ahmed, A. I., and Ibrahim, A. A. (2023). Hydrophilic candle wastes microcapsules as a thermal energy storage material for all-day steam and electricity cogeneration. *Desalination* 550, 116377. doi:10.1016/j.desal.2023.116377

Younis, S. A., Maitlo, H. A., Lee, J., and Kim, K. H. (2020). Nanotechnology-based sorption and membrane technologies for the treatment of petroleum-based pollutants in natural ecosystems and wastewater streams. *Adv. Colloid Interface Sci.* 275, 102071. doi:10.1016/J.CIS.2019.102071

Zabihi, Z., Homayoonfal, M., and Davar, F. (2020). Application of UV irradiation enhanced by CuS photosensitive nanoparticles to mitigate polysulfone membrane fouling. *J. Photochem Photobiol. A Chem.* 390, 112304. doi:10.1016/J.JPHOTOCHEM.2019.112304

Zhan, M., Gwak, G., Choi, B. G., and Hong, S. (2019). Indexing fouling reversibility in forward osmosis and its implications for sustainable operation of wastewater reclamation. *J. Memb. Sci.* 574, 262–269. doi:10.1016/j.memsci.2018.12.074

Zhao, C., Song, T., Yu, Y., Qu, L., Cheng, J., Zhu, W., et al. (2020). Insight into the influence of humic acid and sodium alginate fractions on membrane fouling in coagulation-ultrafiltration combined system. *Environ. Res.* 191, 110228. doi:10.1016/J.ENVRES.2020.110228

Zhao, C., Zhou, J., Yan, Y., Yang, L., Xing, G., Li, H., et al. (2021). Application of coagulation/flocculation in oily wastewater treatment: A review. *Sci. Total Environ.* 765, 142795. doi:10.1016/J.SCITOTENV.2020.142795

Zhao, S., Xue, S., Li, L., Ji, C., Li, P., and Niu, Q. J. (2023). A comprehensive evaluation of PVA enhanced polyamide nanofiltration membranes: Additive versus interlayer. *Colloids Surf. A Physicochem Eng. Asp.* 660, 130870. doi:10.1016/j.colsurfa.2022.130870

Zheng, L., Tang, M., Wang, Y., Hou, D., Li, X., and Wang, J. (2022). A novel Cu-BTC@PVA/PVDF Janus membrane with underwater-oleophobic/hydrophobic asymmetric wettability for anti-fouling membrane distillation. *Sep. Purif. Technol.* 299, 121807. doi:10.1016/j.seppur.2022.121807

Zhong, Q., Shi, G., Sun, Q., Mu, P., and Li, J. (2021). Robust PVA-GO-TiO2 composite membrane for efficient separation oil-in-water emulsions with stable high flux. *J. Memb. Sci.* 640, 119836. doi:10.1016/J.MEMSCI.2021.119836

Zolghadr, E., Firouzjaei, M. D., Amouzandeh, G., LeClair, P., and Elliott, M. (2021). The role of membrane-based technologies in environmental treatment and reuse of produced water. *Front. Environ. Sci.* 9. doi:10.3389/fenvs.2021.629767